LIGO Laboratory / LIGO Scientific Collaboration

LIGO- T1000747-v4 *LIGO* 2/2/13

AOS SLC Arm Cavity Baffle
Final Design

Michael Smith, Virginio Sannibale, Niem Nguyen

Distribution of this document:
LIGO Scientific Collaboration

This is an internal working note
of the LIGO Laboratory.

California Institute of Technology
LIGO Project – MS 18-34
1200 E. California Blvd.
Pasadena, CA 91125
Phone (626) 395-2129
Fax (626) 304-9834
E-mail: info@ligo.caltech.edu

Massachusetts Institute of Technology
LIGO Project – NW22-295
185 Albany St
Cambridge, MA 02139
Phone (617) 253-4824
Fax (617) 253-7014
E-mail: info@ligo.mit.edu

LIGO Hanford Observatory
P.O. Box 159
Richland WA 99352
Phone 509-372-8106
Fax 509-372-8137

LIGO Livingston Observatory
P.O. Box 940
Livingston, LA 70754
Phone 225-686-3100
Fax 225-686-7189

http://www.ligo.caltech.edu/

Table of Contents

Table of Figures

Table of Tables

CHANGE LOG

Date, version	Summary of Changes
V5	• Answers to FDR committee • Wide Angle Scattering from Photon Calibrator Support Structure

1 INTRODUCTION

1.1 Final Design Review Checklist

1.1.1 Final requirements – any changes or refinements from PDR?

T070061-v1-D Stray light Control Design Requirements, was revised to add the requirement for a photo detector array around ACB opening for assisting in the initial pointing of the Arm Length Stabilization beams.

1.1.2 Resolutions of action items from SLC PDR

Refer to: LIGO-L0900119-v1

ISI "0" (HEPI) motion

Please assess the stray light noise estimates with these more realistic inputs for those items being attached to the BSC ISI stage 0.

Ans: See 4

How much isolation is needed for each of the six DOF? Has the proposed design been evaluated for each of these DOF?

Ans: The design was evaluated for the horizontal DOF, which is the worst case.

Lower BRDF Material for Baffles

We suggest the team consider a lower-BRDF material for the more critical baffles, and in particular suggest looking at the electro-static frit black-enameled steel as an option that would give better optical performance.

Ans: We will use black porcelainized steel baffles; See 4.

Viton O-Ring Suspension

Review the tests that have been carried out with the Viton o-ring suspension (is there a report available?).

Ans: The o-ring suspension has been replaced with a maraging steel blade spring that suspends the Baffle from a flexible wire. The baffle is damped with eddy-current damping magnets moving against a fixed copper plate mounted to the down tube of the suspension assembly.

Suspension Internal Modes

•Anything connected to ISI stage 0 should be as light as possible and have body modes no higher than several Hertz (to avoid being problematic for the ISI controls). We suspect the o-ring mount proposed is too stiff in some degrees-of-freedom. Have you considered a multi-wire suspension instead, using coil springs, e.g., for vertical compliance? (seems to us something like this would be easier to install and adjust as well)

Ans: The pendulum mode of the suspended baffle is 1.6 Hz. The internal mode of the suspension structure that is mounted to the ISI stage 0 is > 30 Hz; see 3.4.2.

Earthquake Stops

Tell us more about how the EQ stops are to be mounted to the chamber.

Ans: The earthquake stops consist of travel-limiting rods mounted to the large down-tube that holds the eddy-current copper damping plates, which mounts to the ISI Stage 0--see 3.3.1. The rods restrain the motion of the suspended baffle in three axes.

Un-baffled Light

What happens to the scattered light that passes between the arm cavity baffle ID and the OD of the test mass?

Ans: This annular beam of scattered light is allowed to scatter from the SUS structure and eventually from the chamber walls. It will not cause excessive displacement noise.

Shape of Arm Cavity Baffle

Given the round shapes of the test masses and the manifolds, is there merit to a round arm cavity baffle, rather than square?

Ans: No. The efficient light trapping by the louver shape of the baffle structure requires a rectangular shape.

1.1.3 Subsystem block and functional diagrams

See section 2.

1.1.4 Final Parts Lists and Drawing Package (assembly drawings and majority of remaining drawings)

E1000674_AdLIGO_ASO_BOM_SLC Arm Cavity Baffle Box Final Assy-v1
E1000880 BOM_ACB 1 hole left no QPD
E1000879 BOM_ACB 1 hole right no QPD
E1000878 BOM_ACB 1 hole left QPD
E1000877 BOM_ACB 1 hole right QPD

1.1.5 Final specifications

E0900023-v10_Manufacturing Process Spec for Cantilever Spring Blades

E0900364-v7 LIGO Metal in Vacuum

E1100842_Specification_for_Mirror_Finished_(Super_#8)_Stainless_Steel_to_be_used_in_the_LIGO Ultra-High Vacuum System

1.1.6 Final interface control documents

E1000404-v1 ACB Interface in BSC Chambers H1, H2 for Advanced LIGO(2)

D1002870, Flange Layout, Cable Lengths, Bracket Location and Related Input Documents

D1002870, Flange Layout, Cable Lengths, Bracket Location and Related Input Documents

1.1.7 Relevant RODA changes and actions completed

Not applicable

1.1.8 Signed Hazard Analysis

E1000890-v1 ACB Hazard Analysis

1.1.9 Final Failure Modes and Effects Analysis

Not Required

1.1.10 Risk Registry items discussed

None for this subsystem

1.1.11 Design analysis and engineering test data

See 3.4.1 and 3.4.2.

1.1.12 Software detailed design

Not applicable, ISC will handle this.

1.1.13 Final approach to safety and use issues

No operational safety issues

1.1.14 Production Plans For Acquisition Of Parts, Components, Materials Needed For Fabrication

E1000891-v1_ACB production plan.

1.1.15 Installation Plans and Procedures

This will be deferred until after FDR

1.1.16 Final hardware test plans

- Tests of porcelainized witness samples: ball drop test, visual inspection

  Witness samples taken during each furnace run for porcelainizing the baffle parts will be subjected to a visual inspection and to a standard ball drop test to determine if the adhesion of the porcelain material is sufficient.

- FTIR tests of as-porcelainized parts

  A representative selection of porcelainized baffle parts from each furnace run will be swabbed and a proper FTIR sample collected for subsequent contamination evaluation.

- Blade stiffness measurement

  See E1000892 Arm Cavity Baffle Fabrication, Installation, and Test Plan

- Suspended baffle balancing before installation

  See E1000892-v1 Fabrication, Installation, and Test Plan

1.1.17 Final software test plans

Not applicable, ISC will handle this.

1.1.18 Cost compatibility with cost book

See E1000891-v1_ACB production plan.

1.1.19 Fabrication, installation and test schedule

See E1000892-v1 Fabrication, Installation, and Test Plan

1.1.20 Lessons Learned Documented, Circulated

1.1.20.1 Porcelainizing

In order to maintain the flatness and avoid warping of flat porcelainized parts during the baking process in the continuous feed furnace, the parts must be suspended in such a way that the forces of gravity act in the plane of the part.

Fabricated non-planar shapes that have structural integrity are best porcelainized by using a stationary furnace, and placing the pieces so that gravity forces act normal to a plane of symmetry.

1.1.20.2 Clamping to Stage 0

Based on past experience of clamping suspension structures to support tables and FEA models, we believe that the Arm Cavity Baffle upper mounting plate should be clamped to the ISI Stage 0 with as many clamps as feasible, the clamps being as close to the center of the large down-tube for the suspension structure as possible.

1.1.21 Problems and concerns

TBD

1.2 Applicable Documents

E1000674_AdLIGO_ASO_BOM_SLC Arm Cavity Baffle Box Final Assy-v1

D1002870, Flange Layout, Cable Lengths, Bracket Location and Related Input Documents

E0900023-v10_Manufacturing Process Spec for Cantilever Spring Blades

E0900364-v7 LIGO Metal in Vacuum

E1000083-v4_Spec for Enameled Steel Sheet

E1000404-v1 ACB Interface in BSC Chambers H1, H2 for Advanced LIGO(2)

E1000890-v1 ACB Hazard Analysis

E1000891-v1_ACB production plan

E1000892-v1 Fabrication, Installation, and Test Plan

T060073-00 Transfer Functions of Injected Noise

T070061-v1-D Stray light Control Design Requirements

T080064-00 Controlling Light Scatter in Advanced LIGO

T0900269-v2 Stray Light Control (SLC) Preliminary Design

T1000738 SLC Suspension, Magnetic Field Measurements of the Eddy Current Damper

G0900293 Transmon Sensitivity Calculations

2 ARM CAVITY BAFFLE CONFIGURATIONS

Table 1: Arm Cavity Baffle Configurations

IFO	chamber	number of holes	hole location (viewed toward COC)	No of ALS QPDs	no of shielded cables	no of wires per cable	total no of signal wires	no of ground connections	total no of vacuum feed through	Cable Length	Feedthrough
H1	BSC1	1	right	0					0	N/A	
	BSC3	1	left	0					0	N/A	
	BSC9	2	both	8	2	12	24	2	26	230"x2	LIGO-D1003081: Flange Layout – H1 Beam Splitter Chamber 9 (BSC9) ETMX
	BCC10	2	both	8	2	12	24	2	26	165"x2	LIGO-D1003082: Flange Layout – H1 Beam Splitter Chamber 10 (BSC10) ETMY
H2	BSC7	2	both	8	2	12	24	2	26	165"x2	LIGO-D1003086: Flange Layout – H2 Beam Splitter Chamber 7 (BSC7) ITMX
	BSC8	2	both	8	2	12	24	2	26	230"x2	LIGO-D1003087: Flange Layout – H2 Beam Splitter Chamber 8 (BSC8) ITMY
	BSC5	2	right	0					0	N/A	
	BSC6	2	left	0					0	N/A	
L1	BSC1	1	right	4	1	12	12	1	13	165"x2	LIGO-D1003088: Flange Layout – L1 Beam Splitter Chamber 1 (BSC1) ITMY
	BSC3	1	left	4	1	12	12	1	13	230"x2	LIGO-D1003090: Flange Layout – L1 Beam Splitter Chamber 3 (BSC3) ITMX
	BSC4	1	right	4	1	12	12	1	13	230"x2	LIGO-D1003091: Flange Layout – L1 Beam Splitter Chamber 4 (BSC4) ETMX
	BCC5	1	left	4	1	12	12	1	13	165"x2	LIGO-D1003092: Flange Layout – L1 Beam Splitter Chamber 5 (BSC5) ETMY

2.1 L1 Interferometer

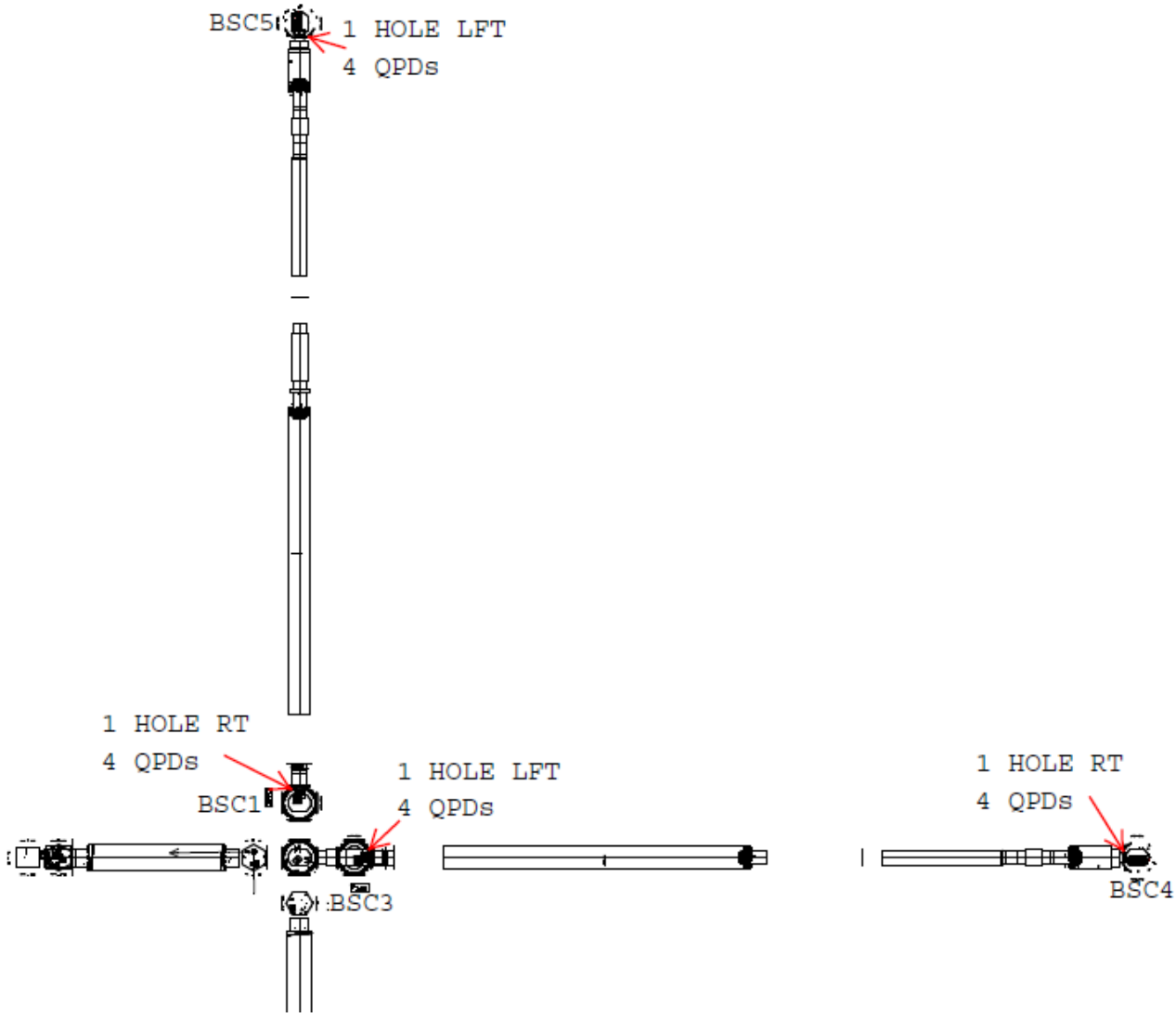

Figure 1: L1 Arm Cavity Baffle Configuration

2.2 H1 Interferometer

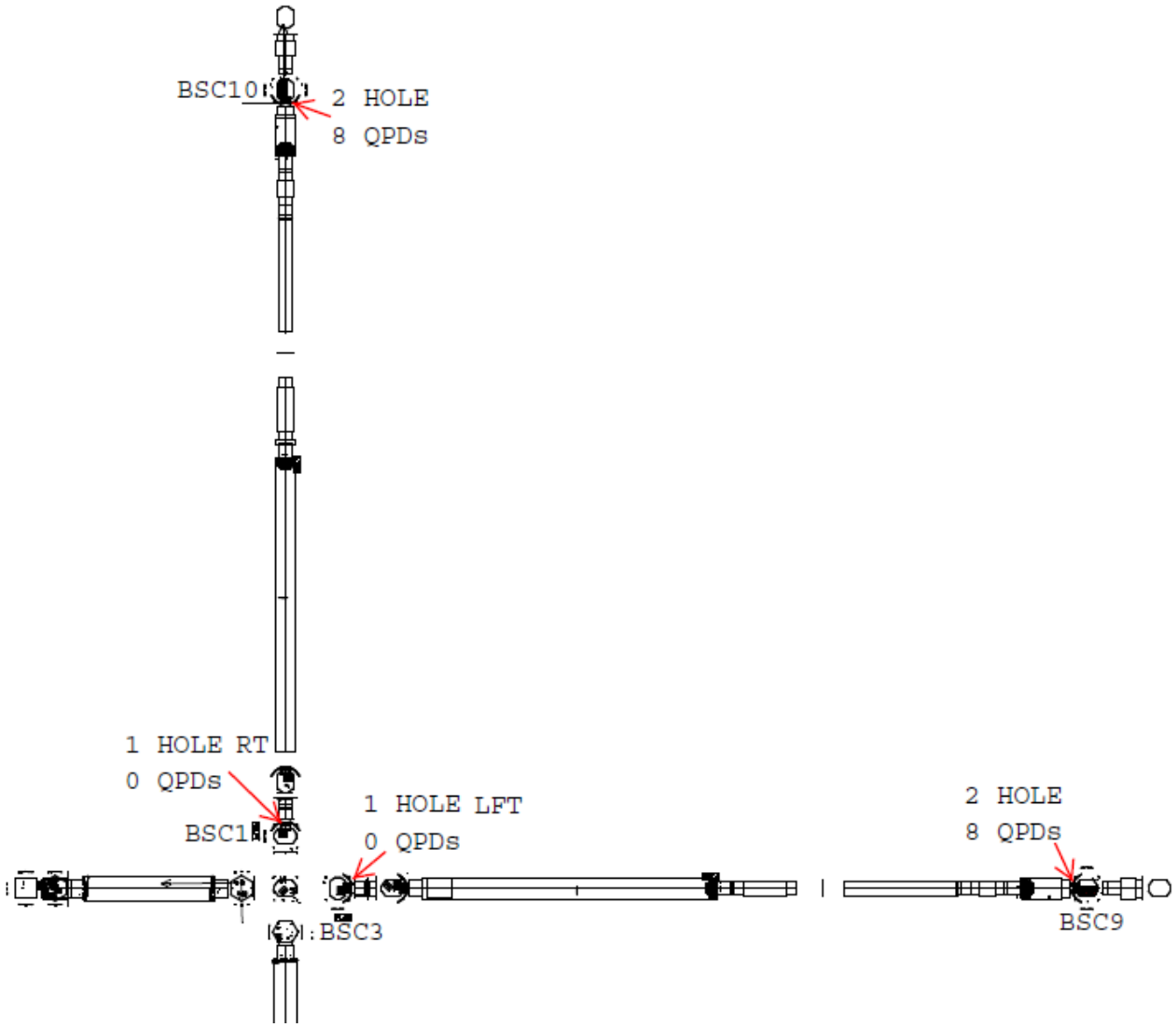

Figure 2: H1 Arm Cavity Baffle Configuration

2.3 H2 Interferometer

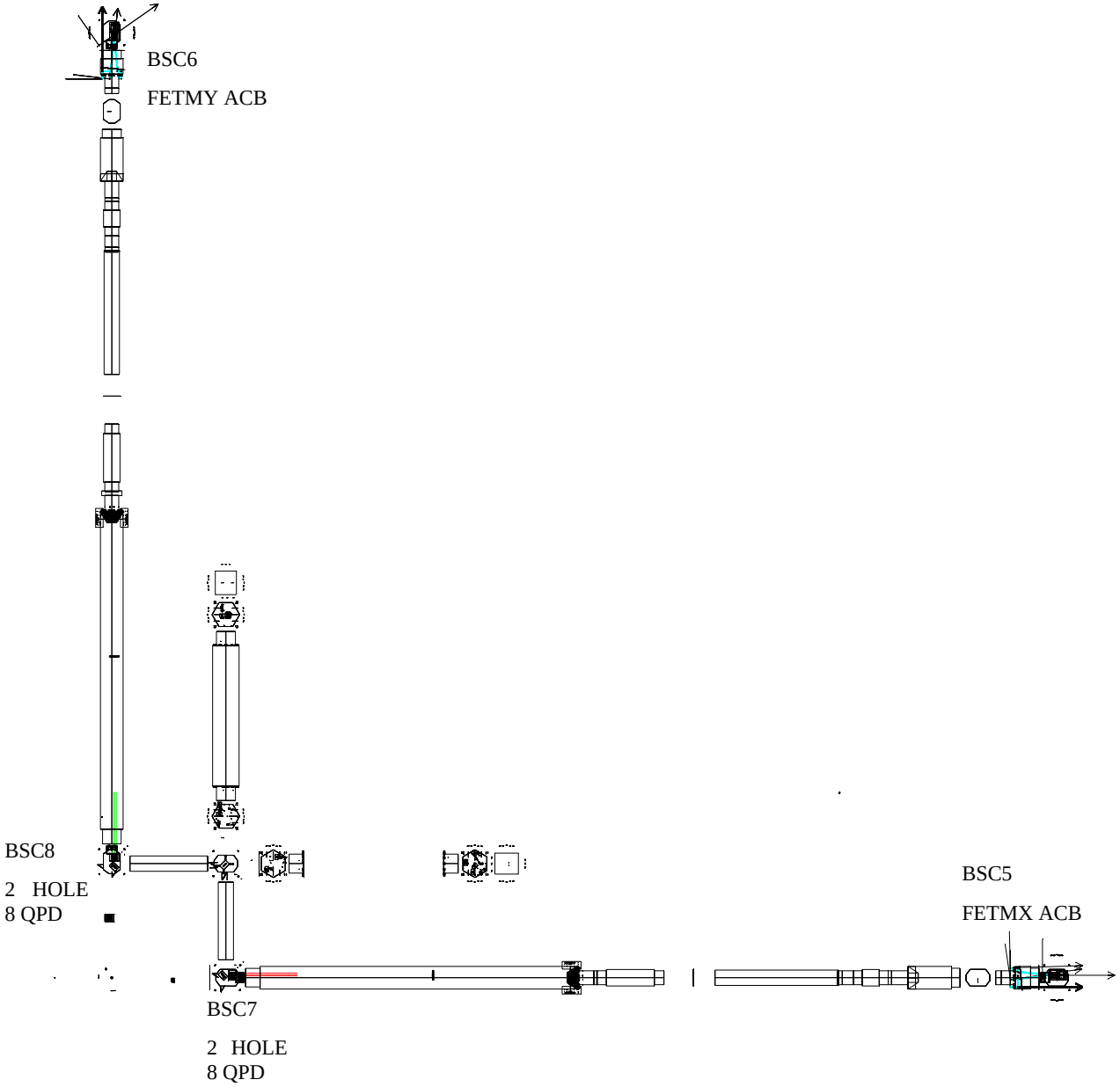

Figure 3: H2 Arm Cavity Baffle Configurations

3 DESCRIPTION OF THE ARM CAVITY BAFFLE

3.1 General Baffle Assembly

The suspended Arm Cavity Baffle interface plate mounts to the ISI Stage 0 in the BSC chamber.

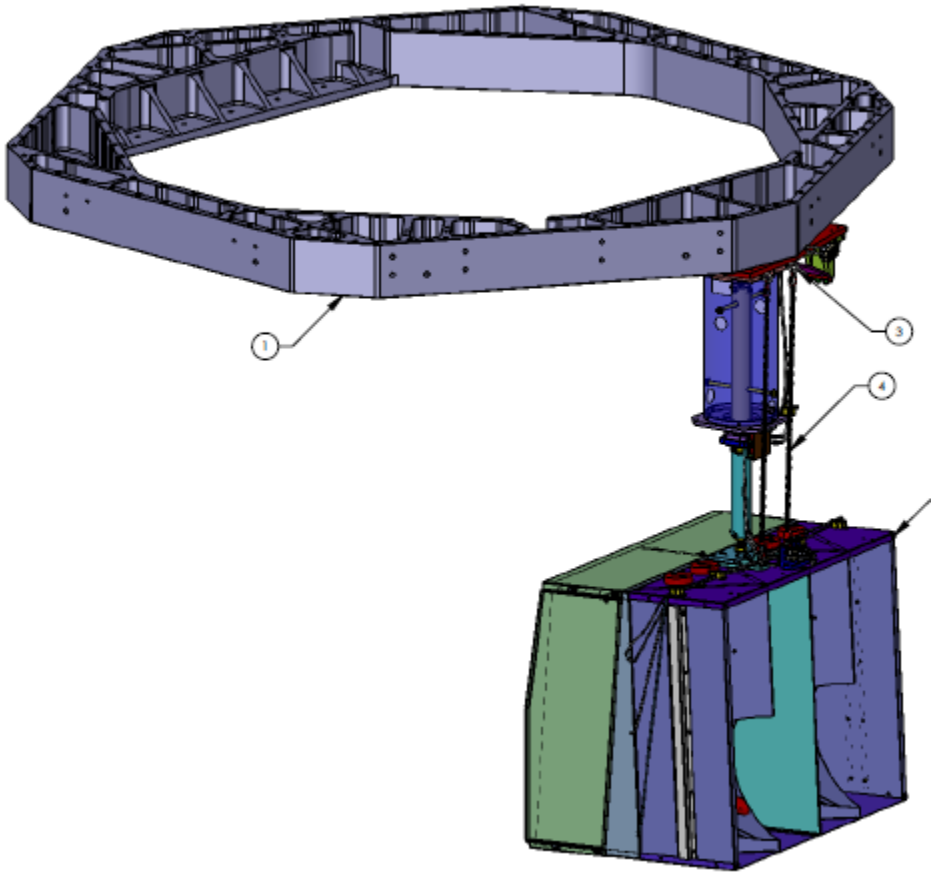

Figure 4: Arm Cavity Baffle Mounting to ISI Stage 0

The mounting locations for the ACB in the various chambers is shown in .

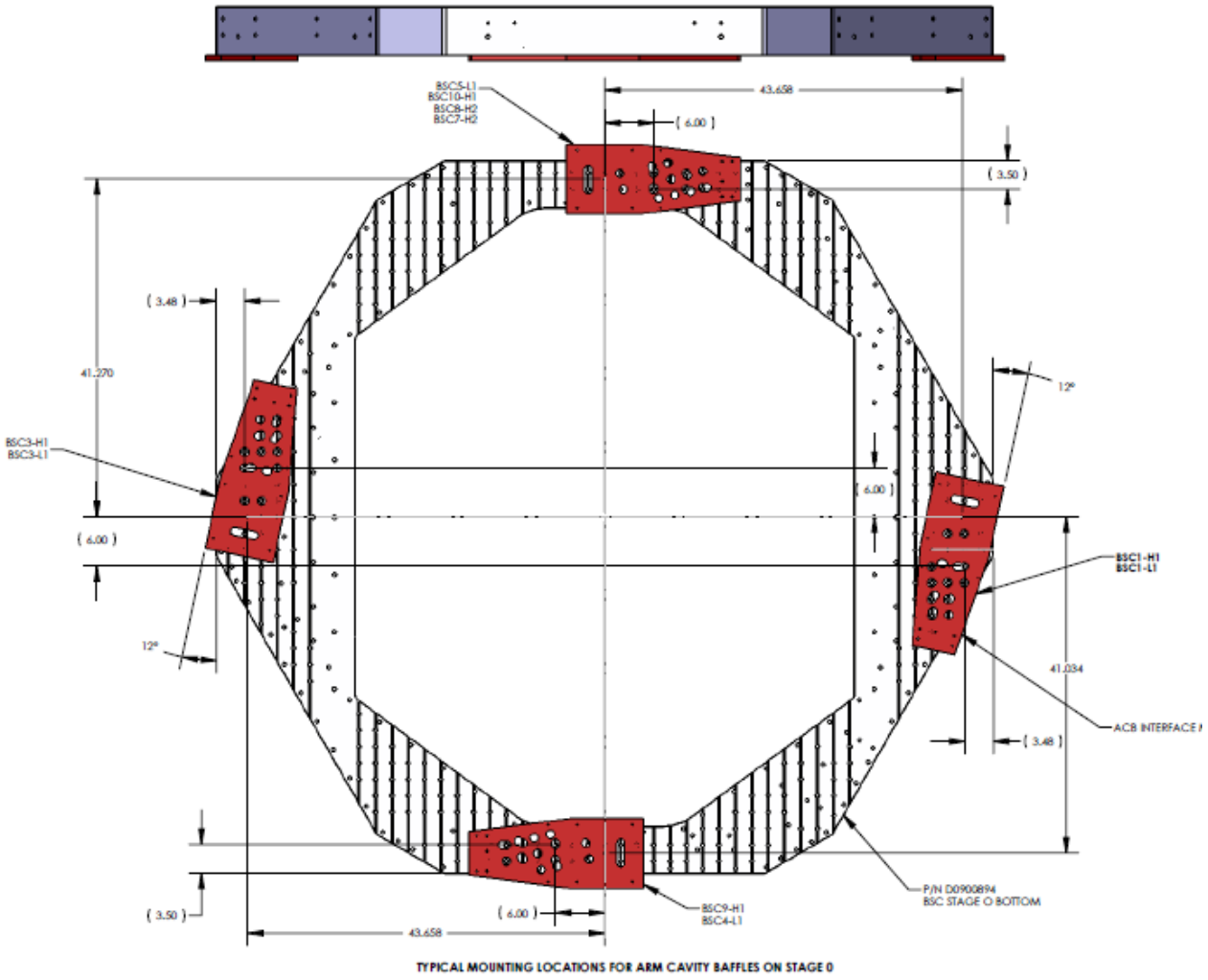

Figure 5: Mounting Locations for ACB in Various BSC Chambers

The down tube supports the eddy current damping mechanism. The light-trapping louver structure is made of oxidized polished stainless steel. The hole diameters in the baffle are slightly larger than the diameter of the ITM and ETM mirrors.

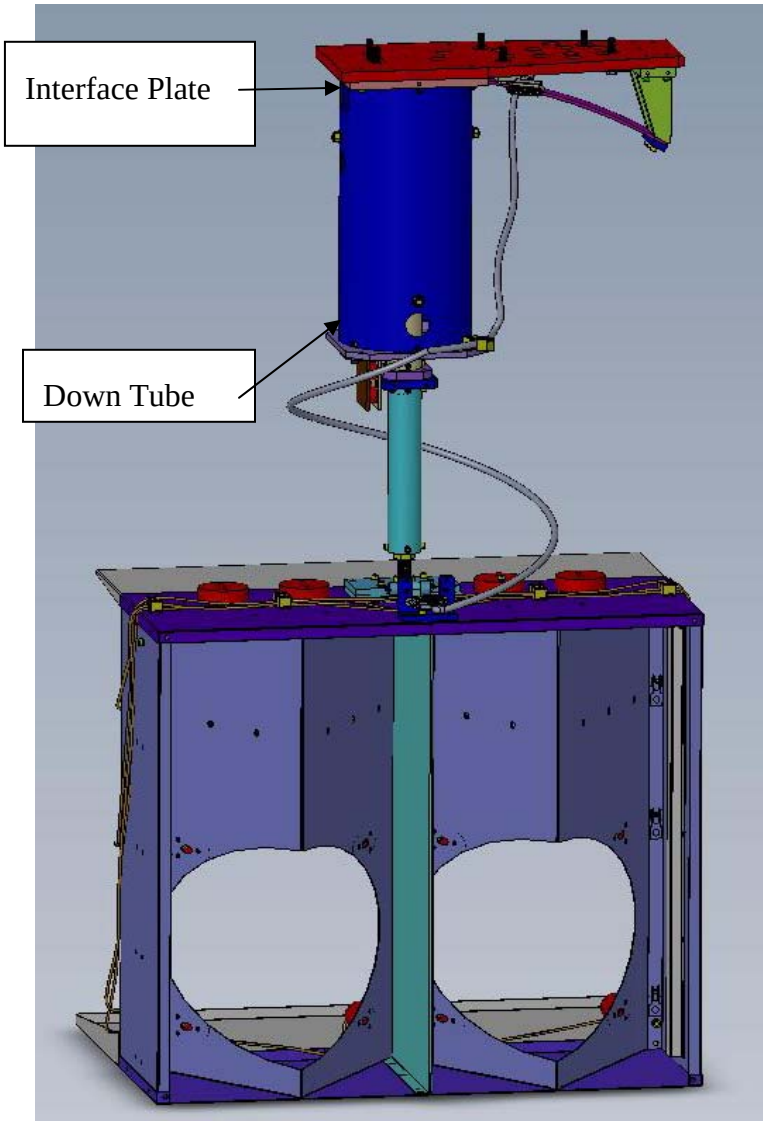

Figure 6: 2-Hole Arm Cavity Baffle Assembly

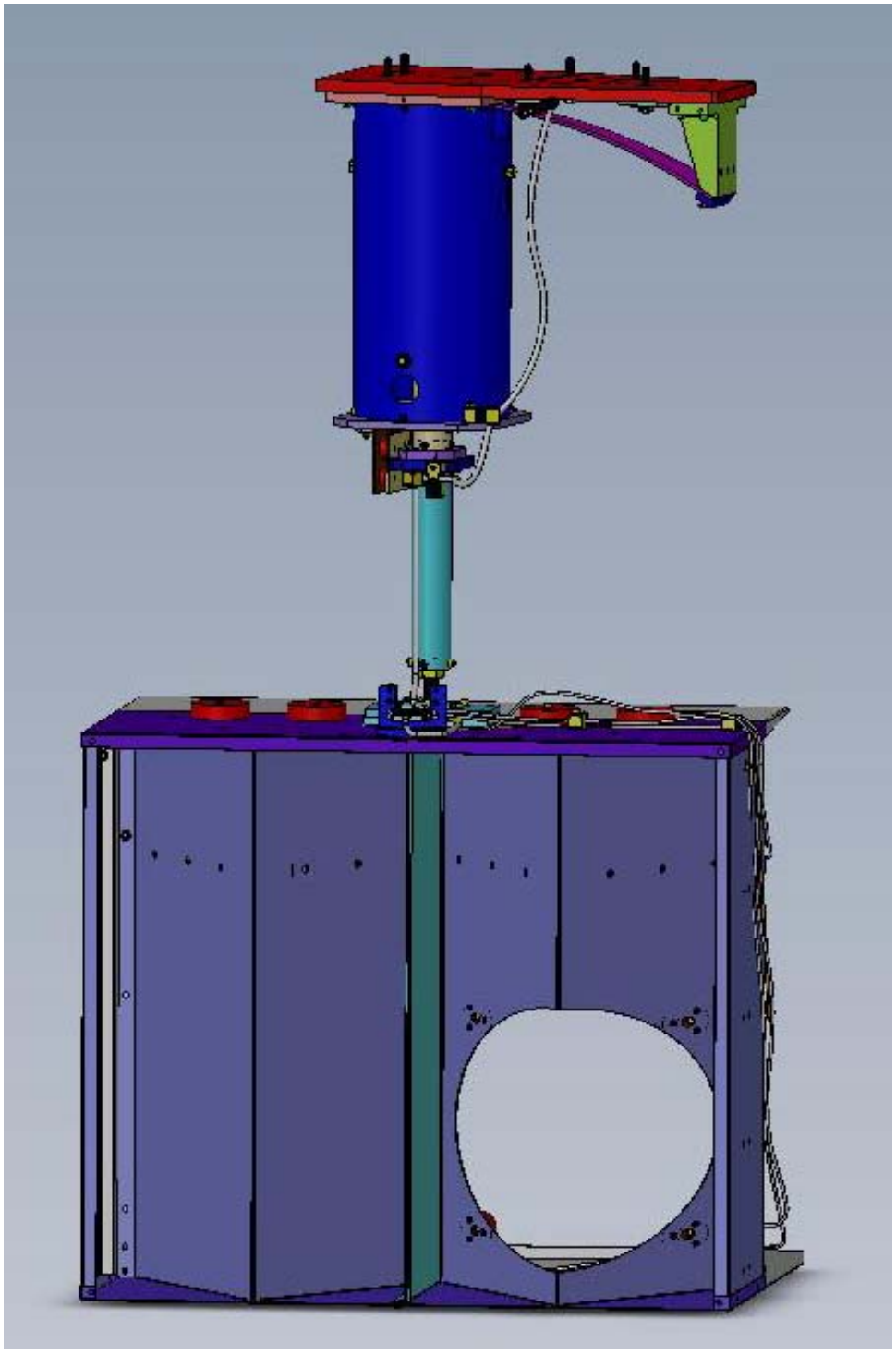

Figure 7: 1-Hole Right, Arm Cavity Baffle Assembly

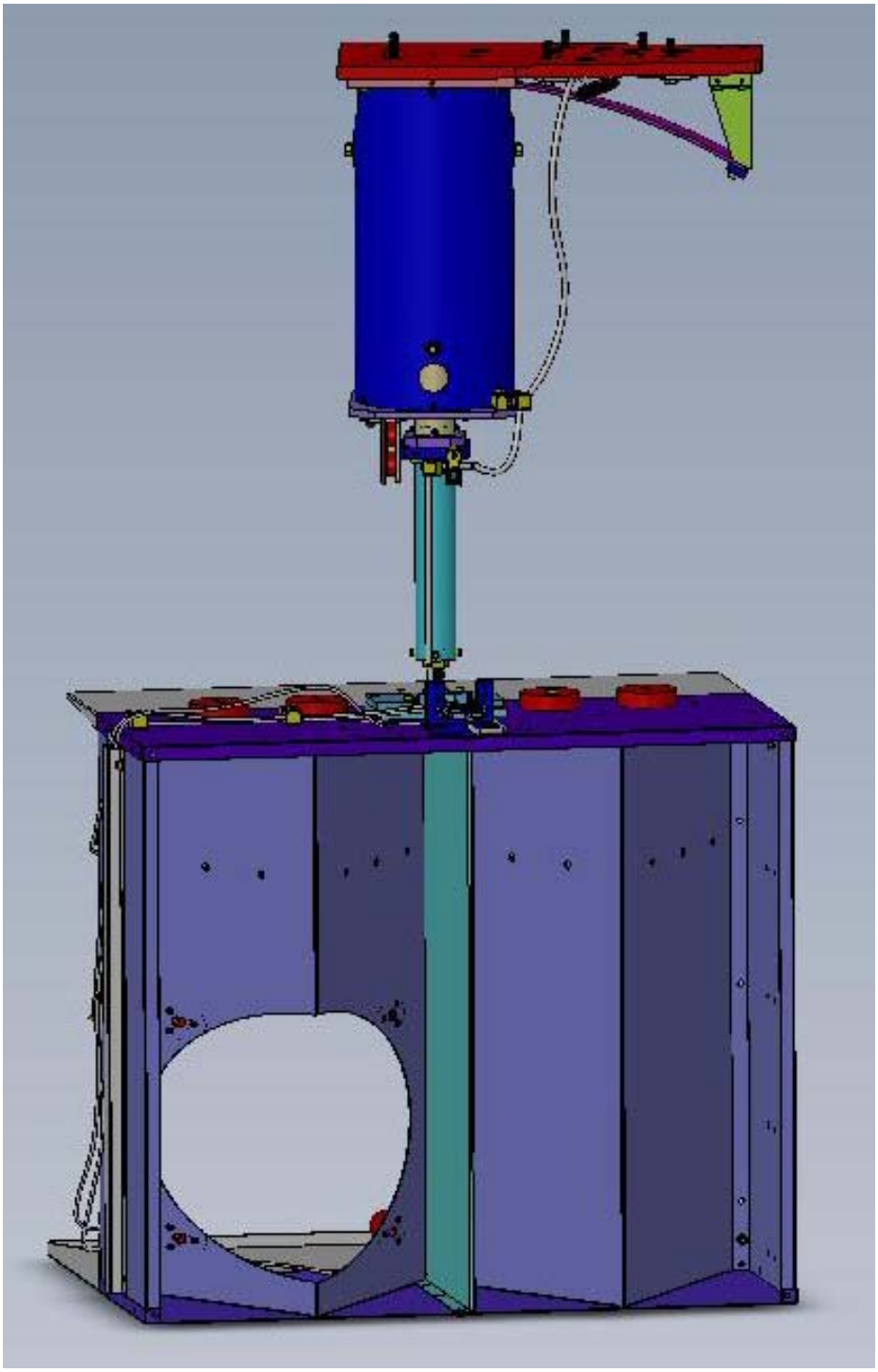

Figure 8: 1-Hole Left, Arm Cavity Baffle Assembly

Table 2: Arm Cavity Baffle Characteristics

Parameter	**Value**
Aperture diameter	346 mm
Outer diameter blockage	>850 mm
Material	Oxidized polished stainless steel
BRDF	<0.05 sr^-1
Reflectivity	<0.05
Total weight	60 kg
Suspended weight	40 kg

Table 3: Arm Cavity Baffle Suspension

Parameter	**Value**
Frame	Aluminum frame
Suspension	Two wire, suspended from HEPI stage “0”
Amplitude response	See 3.4.1
Damping	Q < 100

3.2 H2 FETM ACB Assembly

The H2 ETM arm cavity baffle requires a cut-out to be made in the perimeter of the main beam baffle hole to clear the optical lever beams, as shown in Figure 9; other than that, the H2 FETM ACBs are the same as the single hole baffles without photoconductors.

Figure 10 shows a frontal view of the H2 ETMX mirror in the quad suspension frame, with a sketch of the location of the hole in the FETM ACB, the ACB surface has been rendered transparent in this view. The blue object in the background is the front surface of the TMS telescope frame.

The cut-out in the baffle allows some of the scattered light from the ITM test mass to pass behind the ACB and hit the frame of the TMS telescope, which then scatters into the IFO mode and causes scattered light displacement noise; this noise source is acceptable, as shown in the calculations of Section 4 SCATTERED LIGHT DISPLACEMENT NOISE.

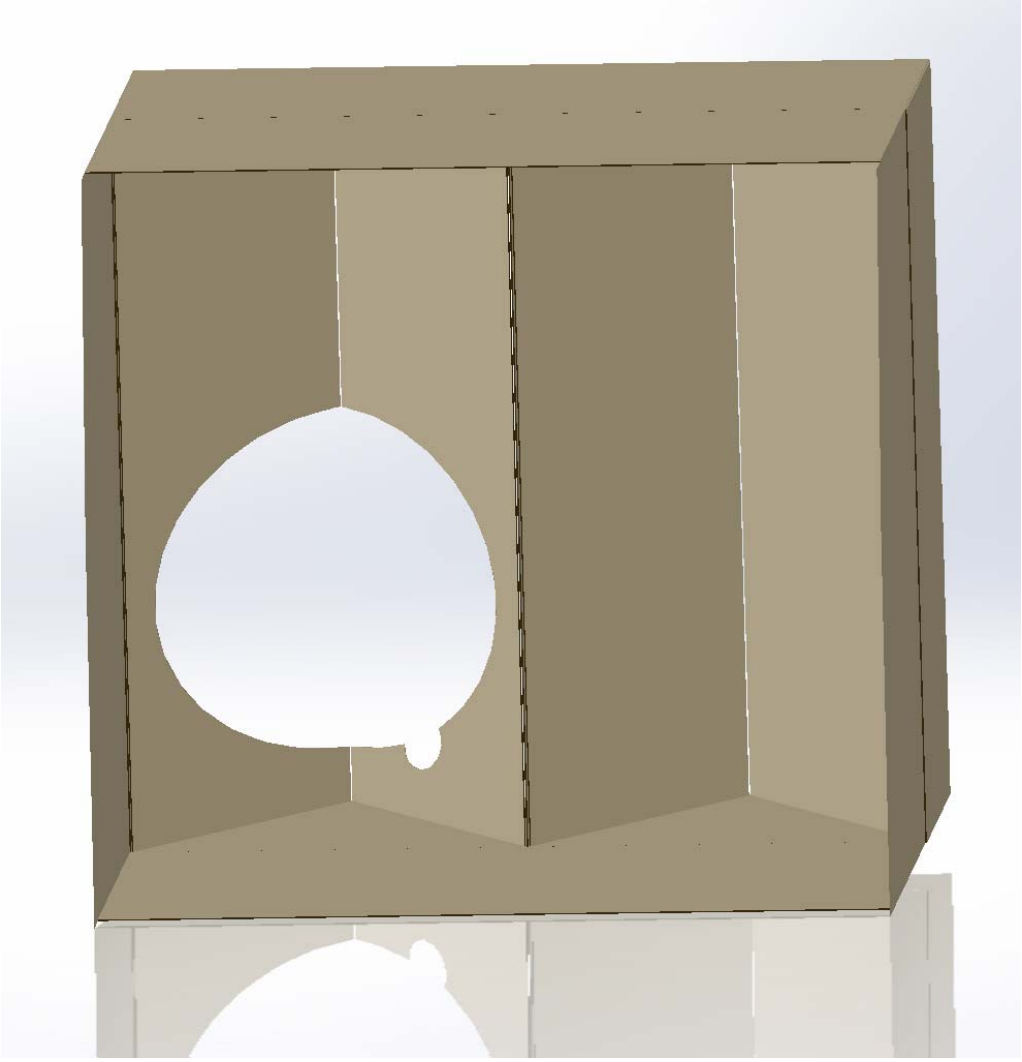

Figure 9: FETMX Arm Cavity Baffle with Cut-out for Optical Lever Beam, H2 BSC5

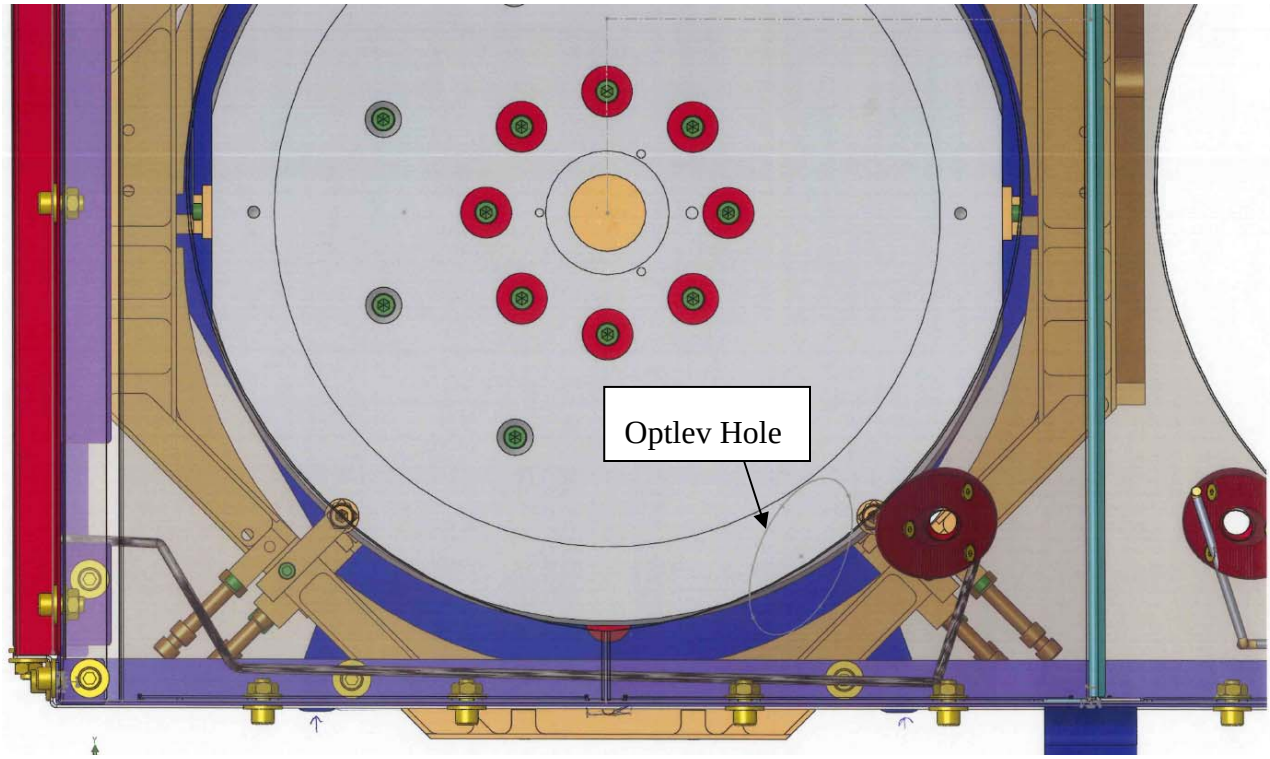

Figure 10: FETMX ACB (made transparent) Showing Sketch of the Location of Optlev Hole

3.3 Requirement to Lift the ACB Out of the Way while Working on Quad Suspension

The Arm Cavity Baffle attaches to the suspension tube with a hinge joint that allows the baffle to be swung away from the quad suspension structure whenever close access to the COC mirror is needed. The wide-angle baffle plates that protrude like shelves from the arm cavity baffle can also be temporarily removed for additional access to the COC mirror.

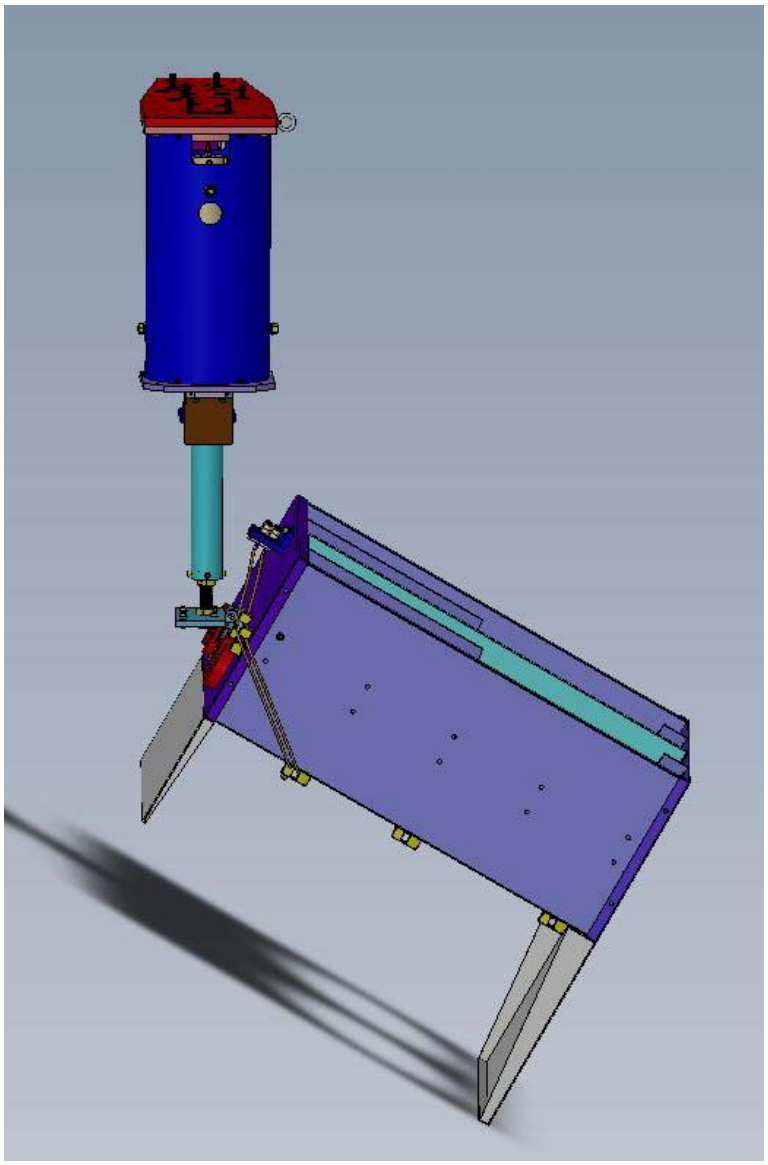

Figure 11: Arm Cavity Baffle Rotated Away from the Quad Suspension

3.3.1 Earthquake Stops

The earthquake stops consist of travel-limiting rods mounted to the large down-tube that holds the eddy-current copper damping plates, which mount to the ISI Stage 0, as shown in Figure 12. The rods restrain the excess motion of the suspended baffle in three axes.

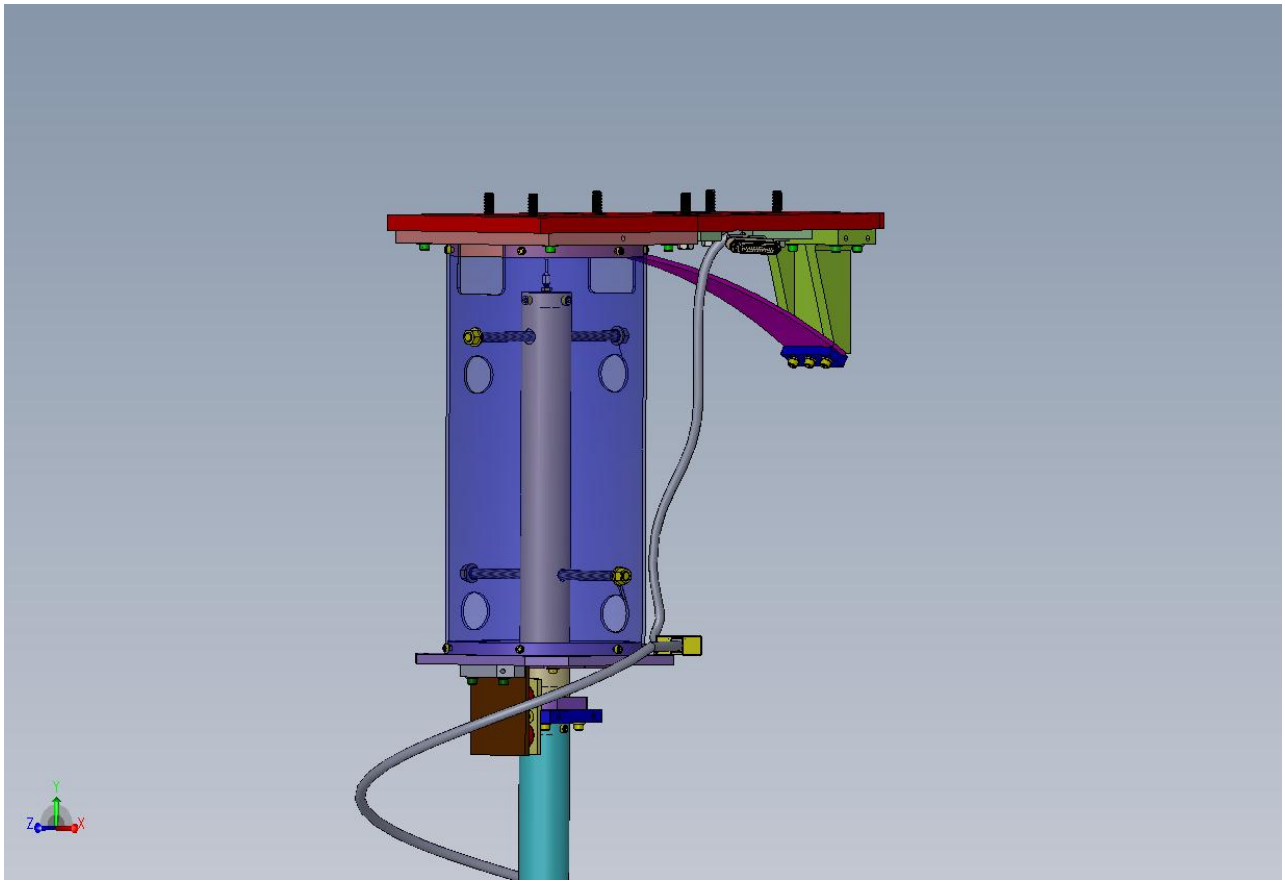

Figure 12: Earthquake Stops

3.4 Arm Cavity Baffle Suspension

3.4.1 Transmissibility Measurements

The measured transmissibilities (green curve) are compared with the damped pendulum analytical model (red curve) in the vicinity of 10 Hz. The actual magnitudes agree reasonably well with the model. Beyond 10 Hz, the amplitude remains approximately constant at the background noise level, except for internal resonances of the baffle suspension.

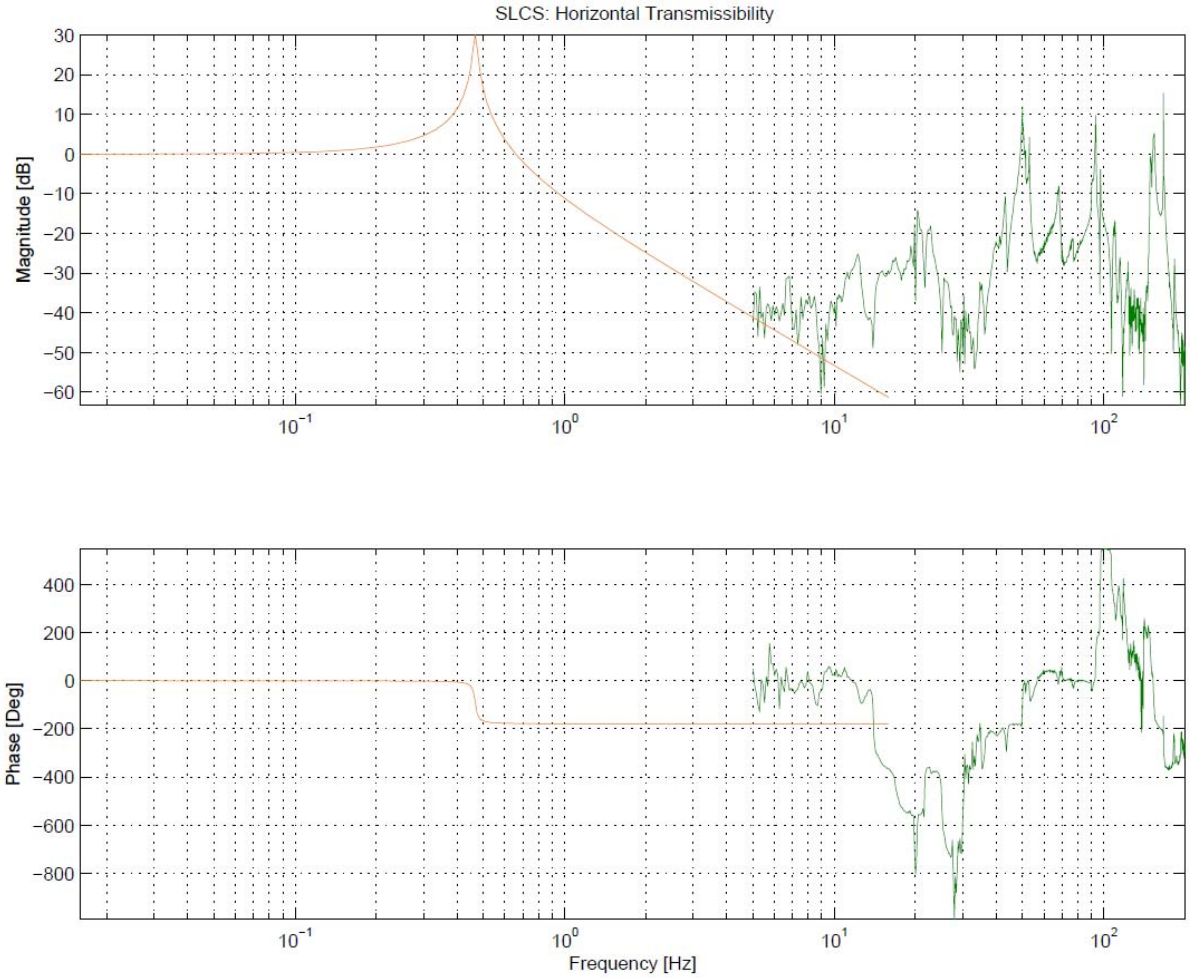
SLCS: Horizontal Transmissibility
Magnitude [dB]
30
20
10
0
−10
−20
−30
−40
−50
−60
10^{-1}
10^{0}
10^{1}
10^{2}
Phase [Deg]
400
200
0
−200
−400
−600
−800
10^{-1}
10^{0}
10^{1}
10^{2}
Frequency [Hz]

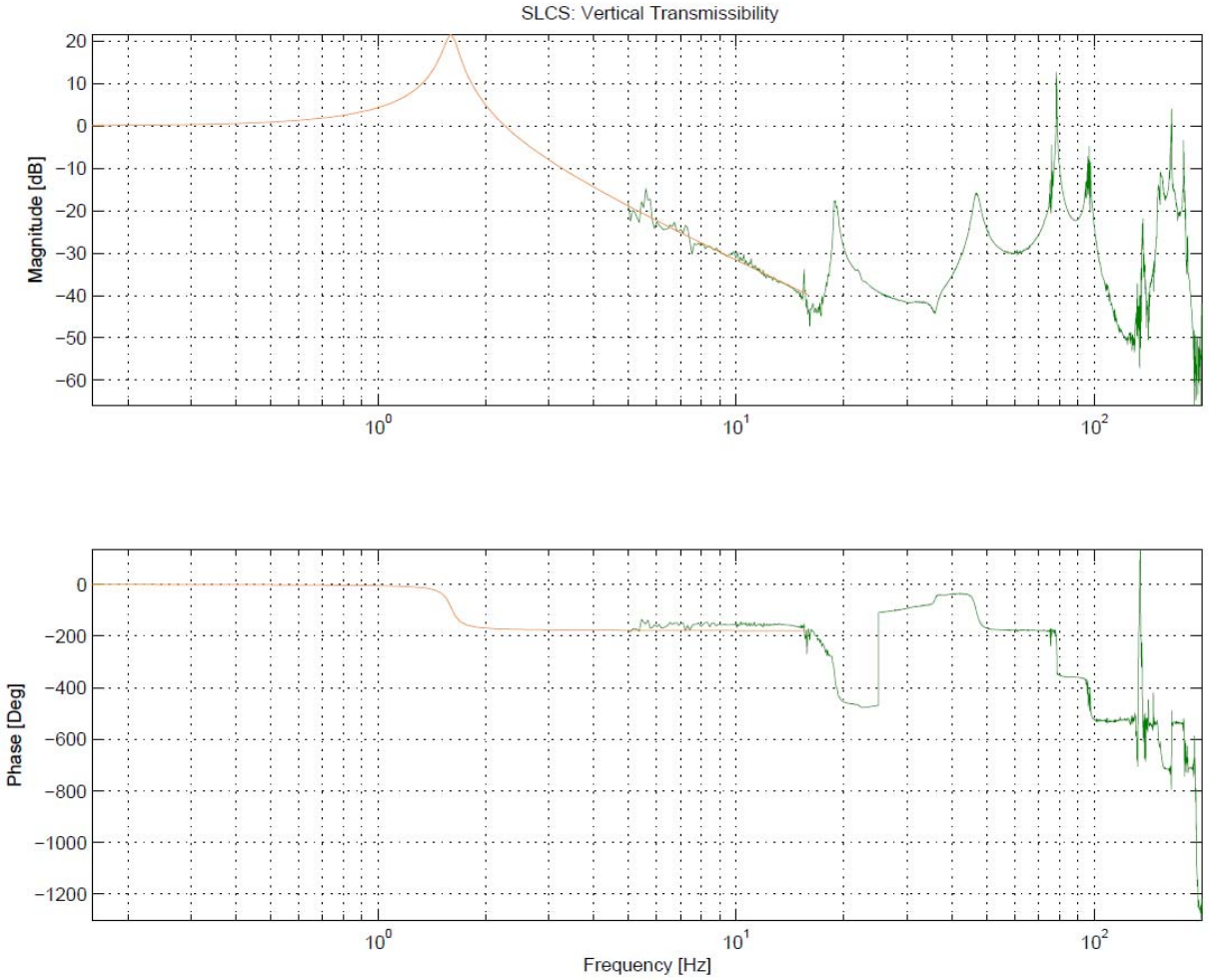

3.4.2 Stray Magnetic Field Measurement

The eddy current damper magnets of the Arm Cavity Baffle are placed > 0.7 m distance from the magnets of the TM SUS magnets, as shown in figure ; the actual distance is 797 mm (the ACB magnet plate will be rotated 90 deg away from the TM SUS in this figure). The interaction of the eddy current damping magnets with the COC suspension magnets was estimated, as described below; see Magnetic Field Measurements.

The results of those measurements and extrapolations from the fit show that the magnetic field spectrum at a distance of 0.7m is estimated to be about 1 pTrms/$\sqrt{}$Hz above 10Hz, a value one order of magnitude lower than the natural magnetic field measured at Hanford. Considering that the expected seismic noise on a Caltech's build third floor is presumably larger than the one at the sites, the spectrum noise is dominated by the instrument noise, and the number of permanent magnets used will be reduced by a factor two, the residual magnetic field spectrum estimation at a distance of 0.7 m is conservative for the following reasons:

1) spectrum used is the one measured using four magnets, and we will use two magnets

2) the distance where the spectrum was extrapolated is 0.7m and the last stage of the quadruple pendulum is further away. The dipole spectrum dies quite fast with the distance (third power)
3) the spectrum is overestimated because the measurement is dominated by the instrument noise above 10 Hz,
4)The seismic noise @ Caltech is probably higher than the ones at the sites.

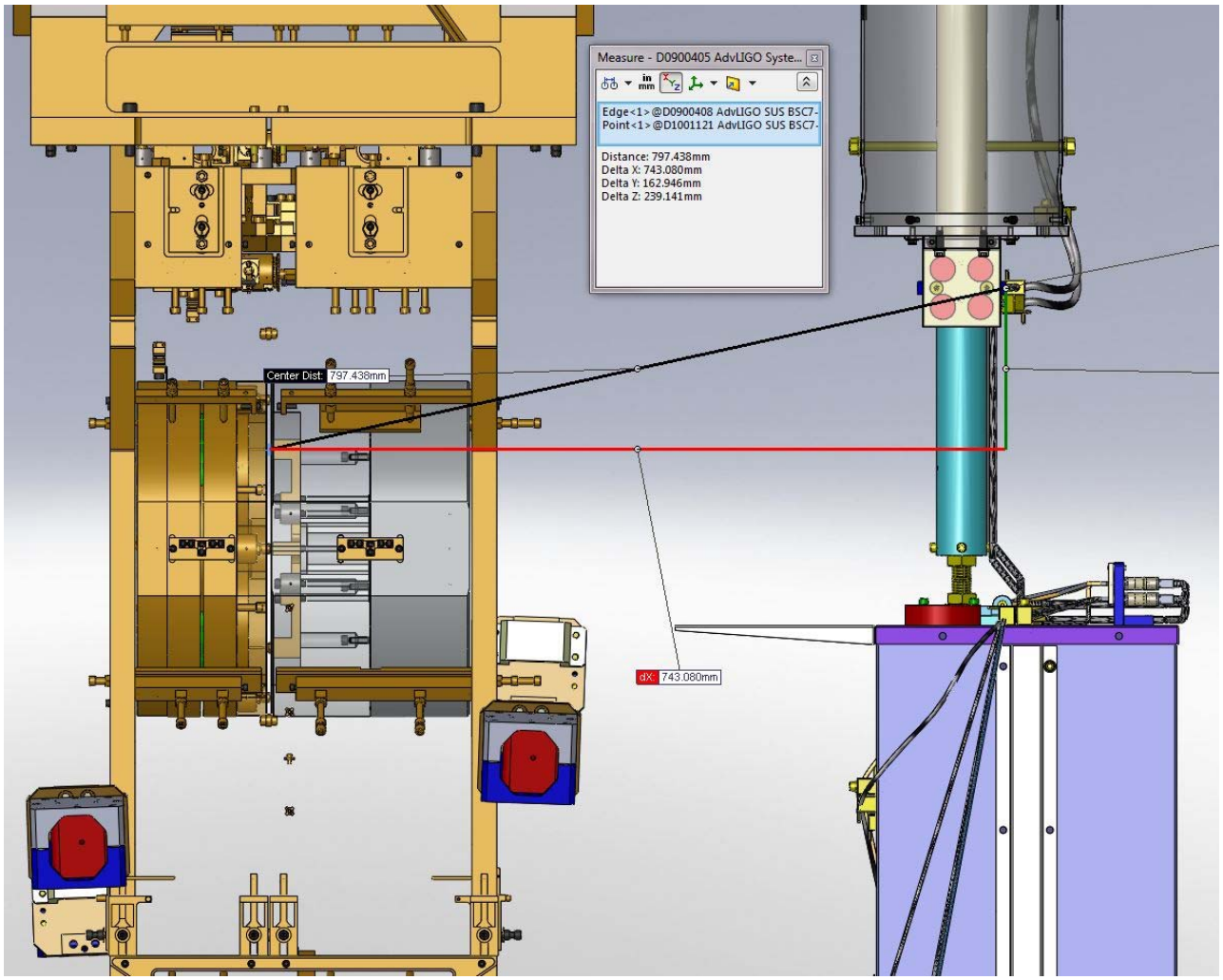

Figure 13: Location of Eddy Current Magnets from the SUS Magnets

, 27-Jan-2011 17:03:09

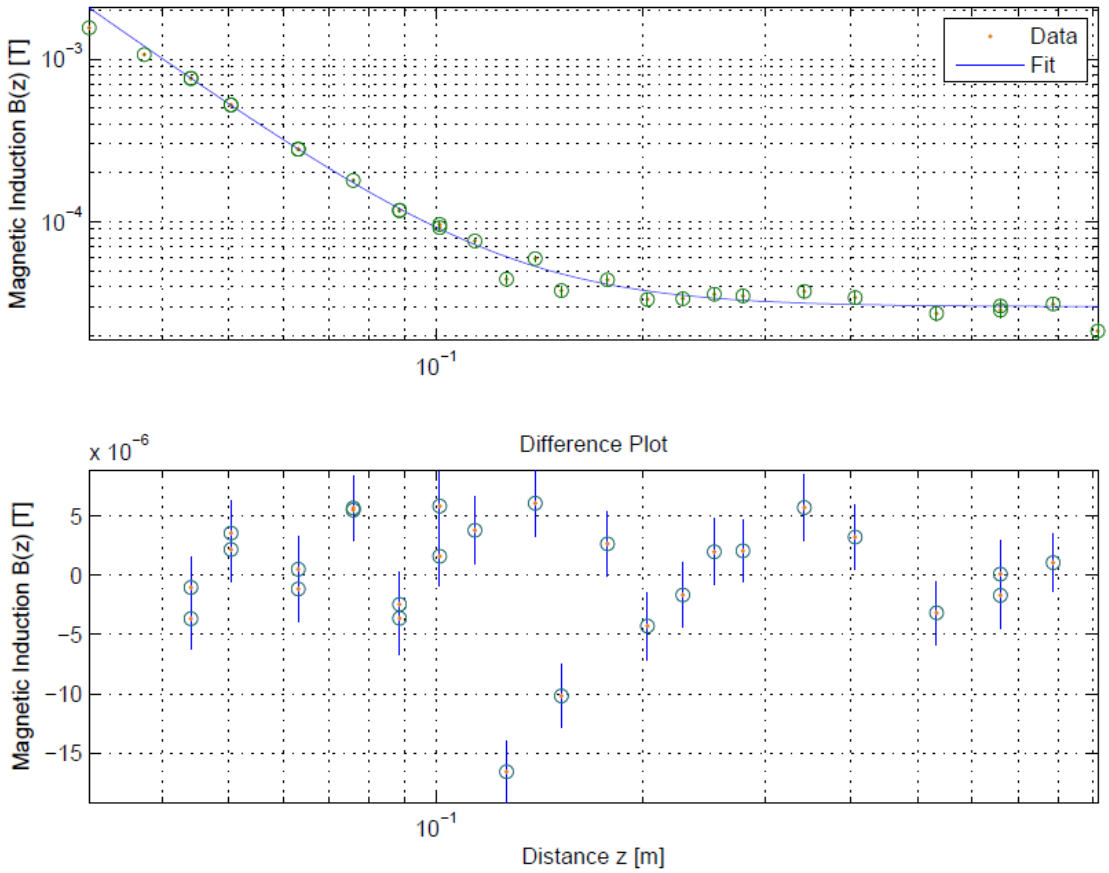


```
Fitting Function:
 y(x)=a*x.^b+c

Parameters:
.       a = ( 6.2744 +- 0.0286 )x10^-8
                        b = -3.00000e+00 (Constant)
.       c = ( 3.019 +- 0.121 )x10^-5
```

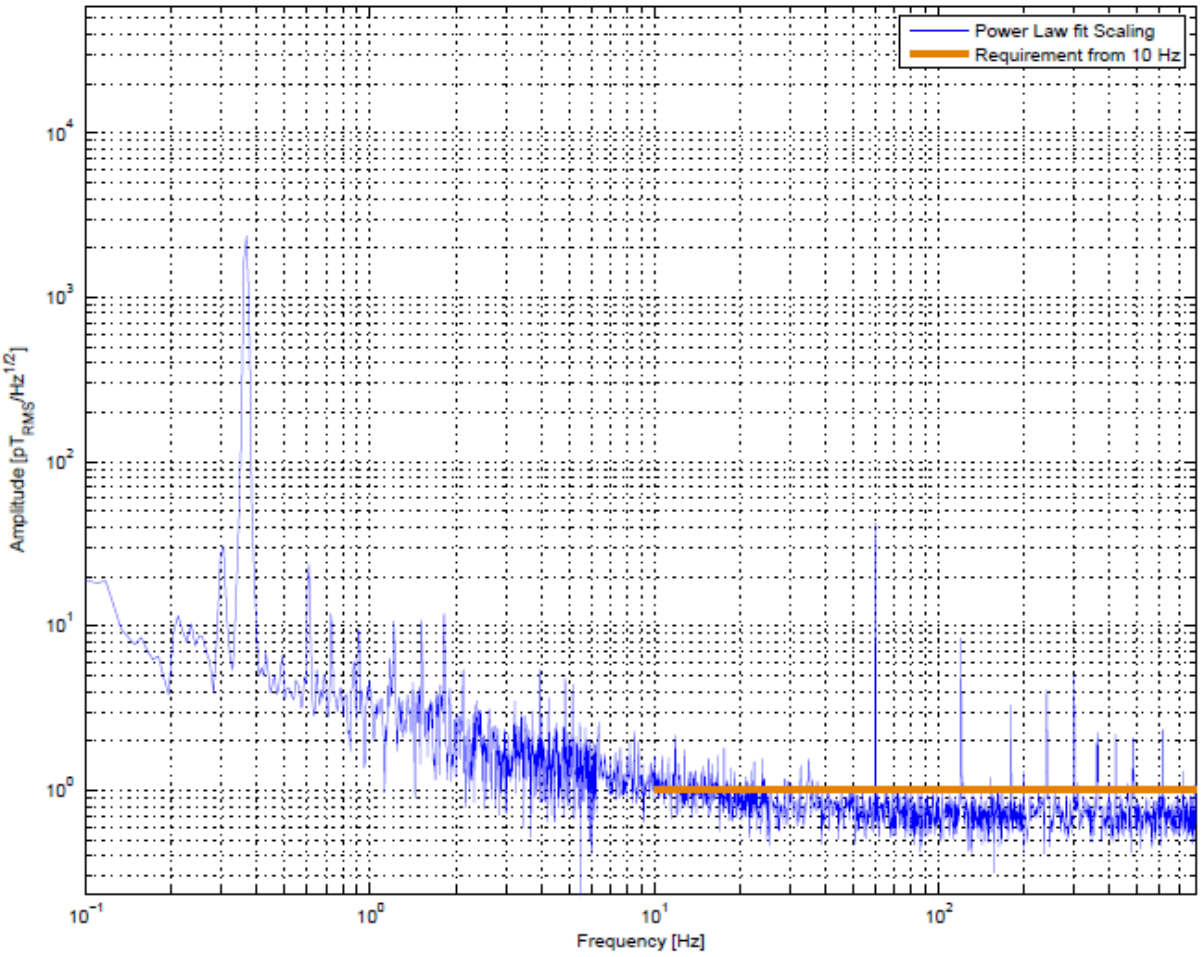

Details of these measurements are reported in [T1000738 SLC Suspension, Magnetic Field Measurements of the Eddy Current Damper].

3.4.3 LASTI Arm Cavity Baffle Suspension Test

The Arm Cavity Baffle Suspension, with a representative dummy load, was installed in the LASTI BSC chamber to test the effect of the baffle suspension internal modes on the transfer function of the ISC control system. The test results are described in

[T1000737 Stray Light Control Suspension, Results of the LASTI Test]
The measurement performed at LASTI on the SLC suspension attached to the ISI stage 0 with adequate damping of the rigid body modes, shows that the Arm Cavity Baffle suspension does not compromise the performance of the ISI Stage 0.

3.5 ALS Photo detector Array

A vacuum compatible ALS photodiode array is placed around the circumference of the Arm Cavity Baffle holes. The photodiodes will be used for lock acquisition by assisting in the initial pointing of the Power Recycling Cavity beam and the ALS beams.

The orientations of the photodetectors for the different configurations of baffles are shown in

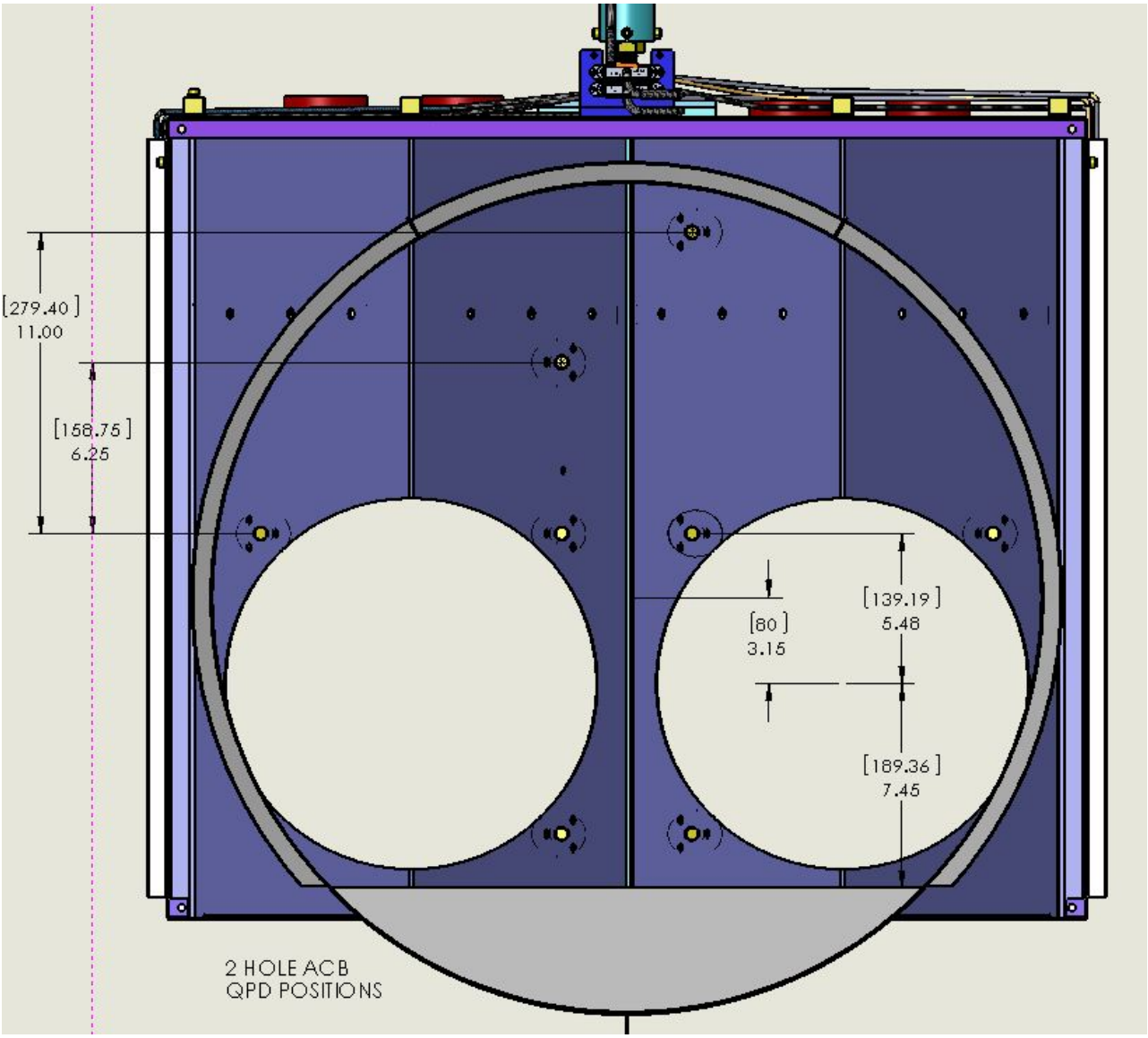

Figure 14: Two-hole, Baffle Photo Detector Orientation

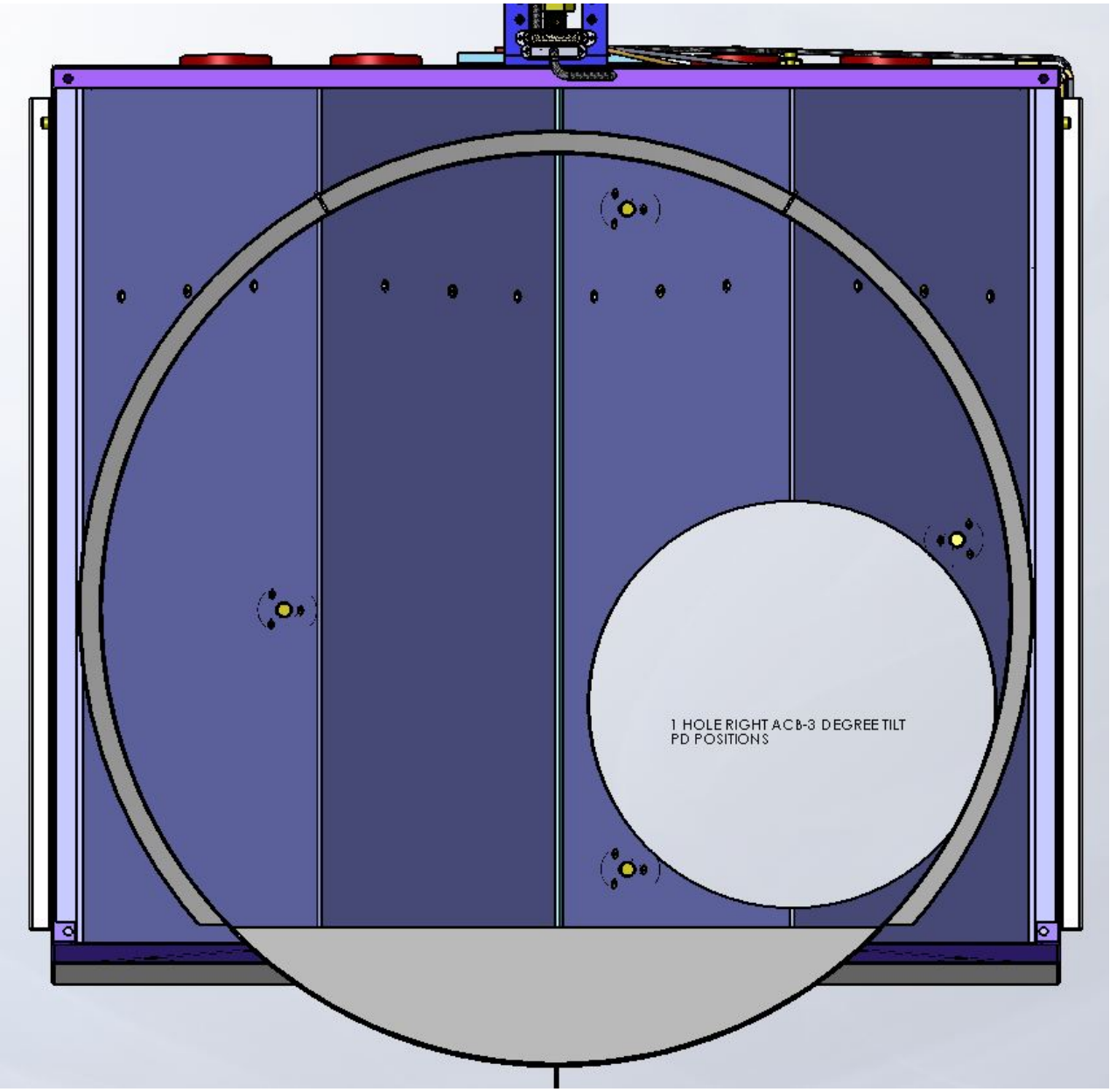

Figure 15: One-hole Right, Baffle Photo Detector Orientation

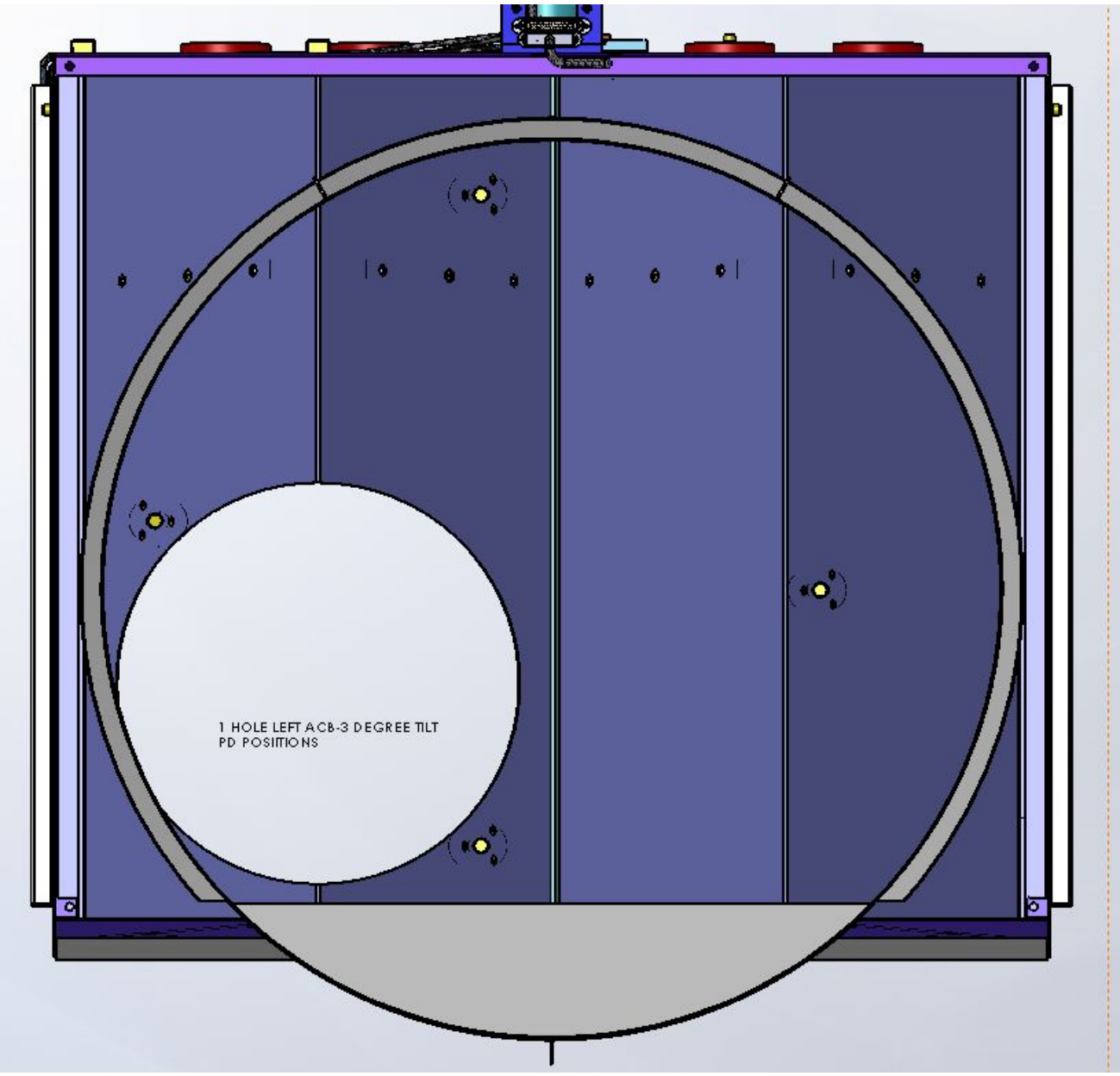

Figure 16: One-hole Left, Baffle Photo Detector Orientation

The photo detector assemblies in their housings are mounted to the back side of the baffle, as shown in Figure 17, using stainless steel flat head screws that are visible from the beam side, with an opening in the baffle that allows only the active photo detector surface to be in the line of sight of the light from the far arm. Electrical cabling attaches to each photo detector, and electrical voltage and signals are carried through the cable to vacuum feed through that allow a connection to racks outside the vacuum chamber.

The Photodiode in the photo detector is from PerkinElmer, YAG-444AH photodiode. It has a circular active area 200 mm^2 and with a 16.0 um diameter. The photodiode is mounted in a TO-36 package.

These are the nominal parameters for the photo detector.

Table 4: ACB Photodiode Parameters

Photodiode Parameters			
Parameter	**Symbol**	**Value**	**Units**
Peak Wavelength	λ	1000	nm
Responsivity	R	0.7	A/W
SLCDiameter	D	16.0	um
Active Area	A	200	mm^2
Diode Capacitance	C	35	pF
Rise/Fall Time	t	5	ns
Dark Current	A	<200	nA
Breakdown Voltage	V	>200	V
Operating Voltage	V	180	V

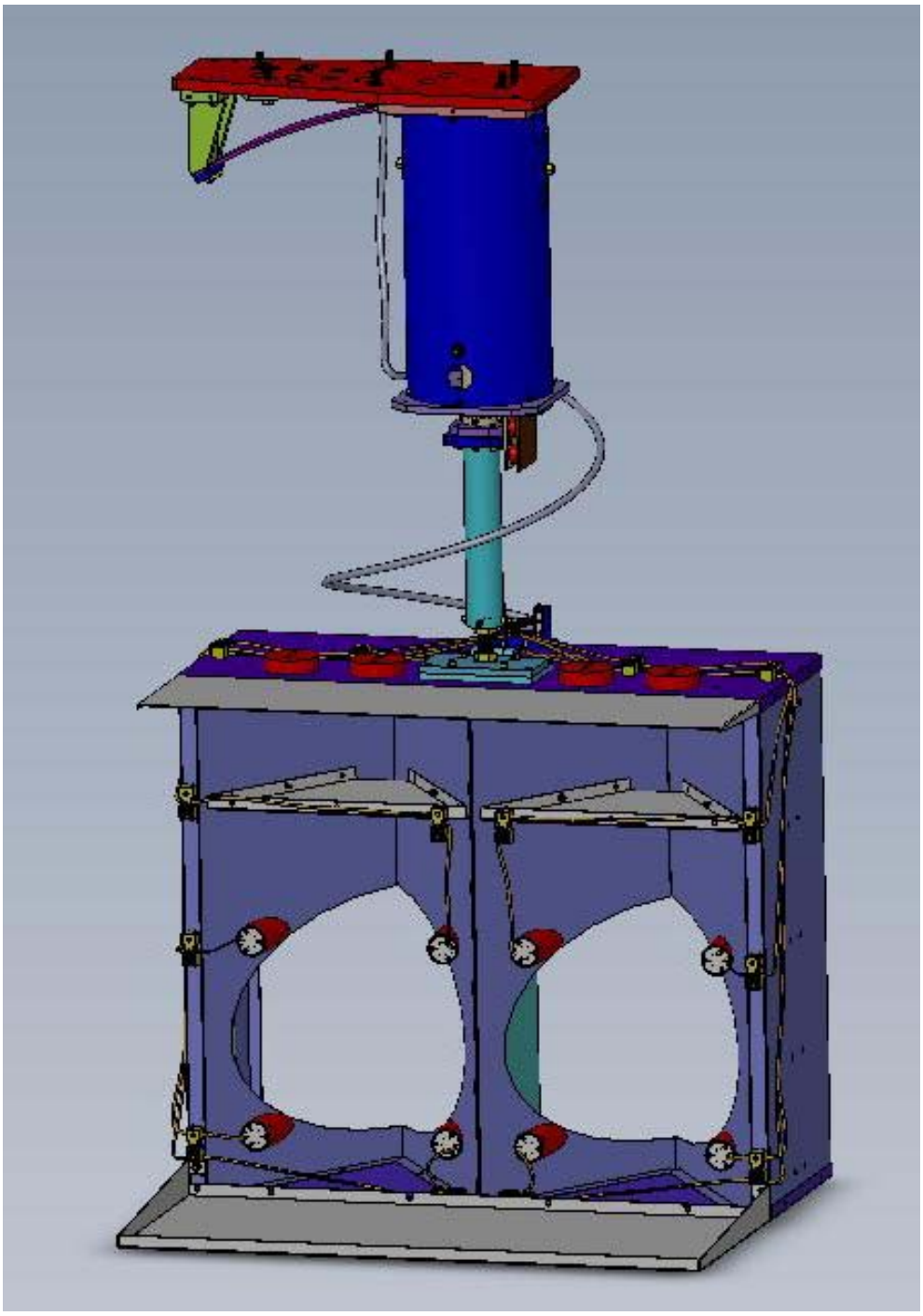

Figure 17: ALS Photodiodes Mounted to Back Side of ACB

The detail of the photo detector assembly is shown in Figure 18.

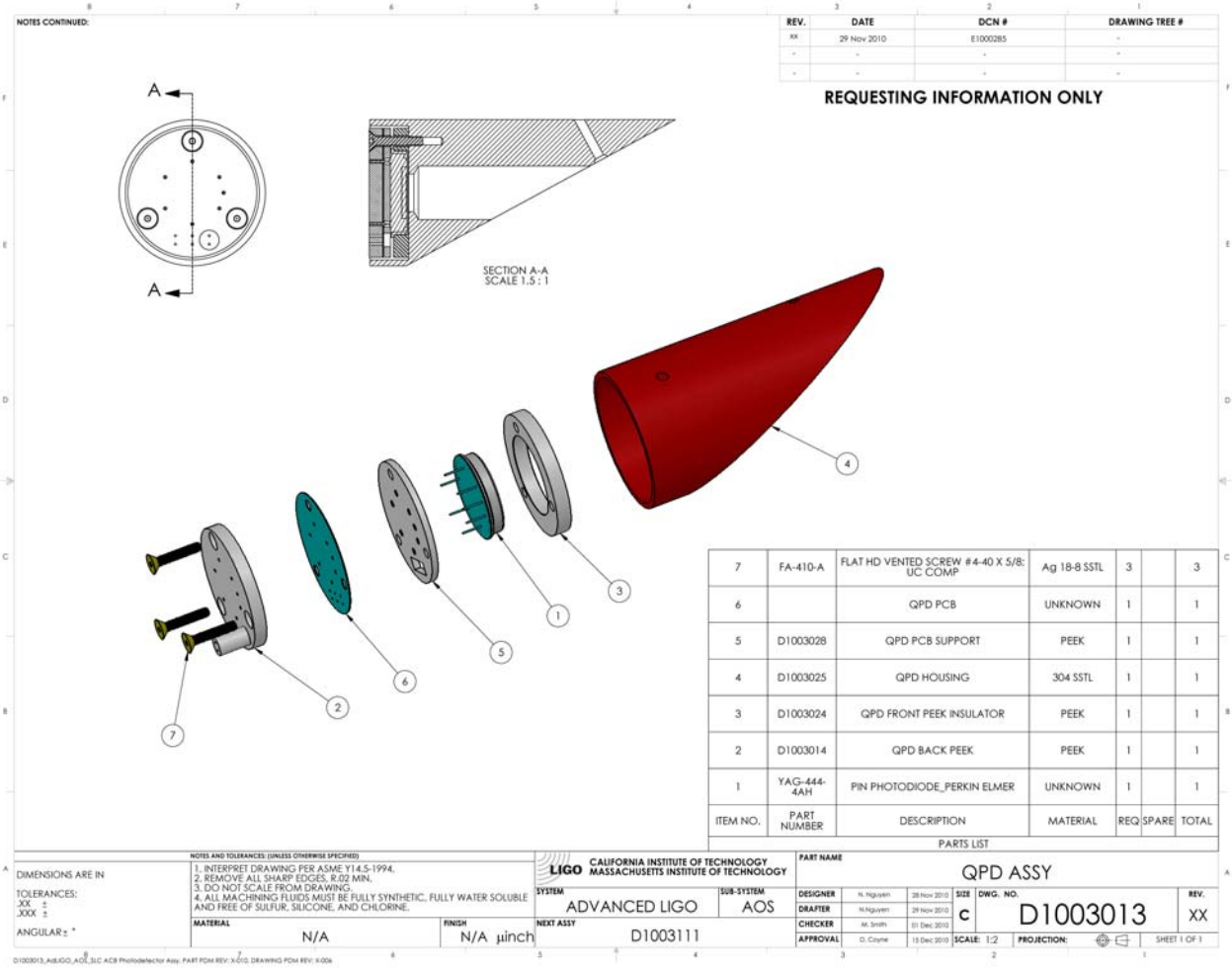

Figure 18: ALS Photo detector Assembly

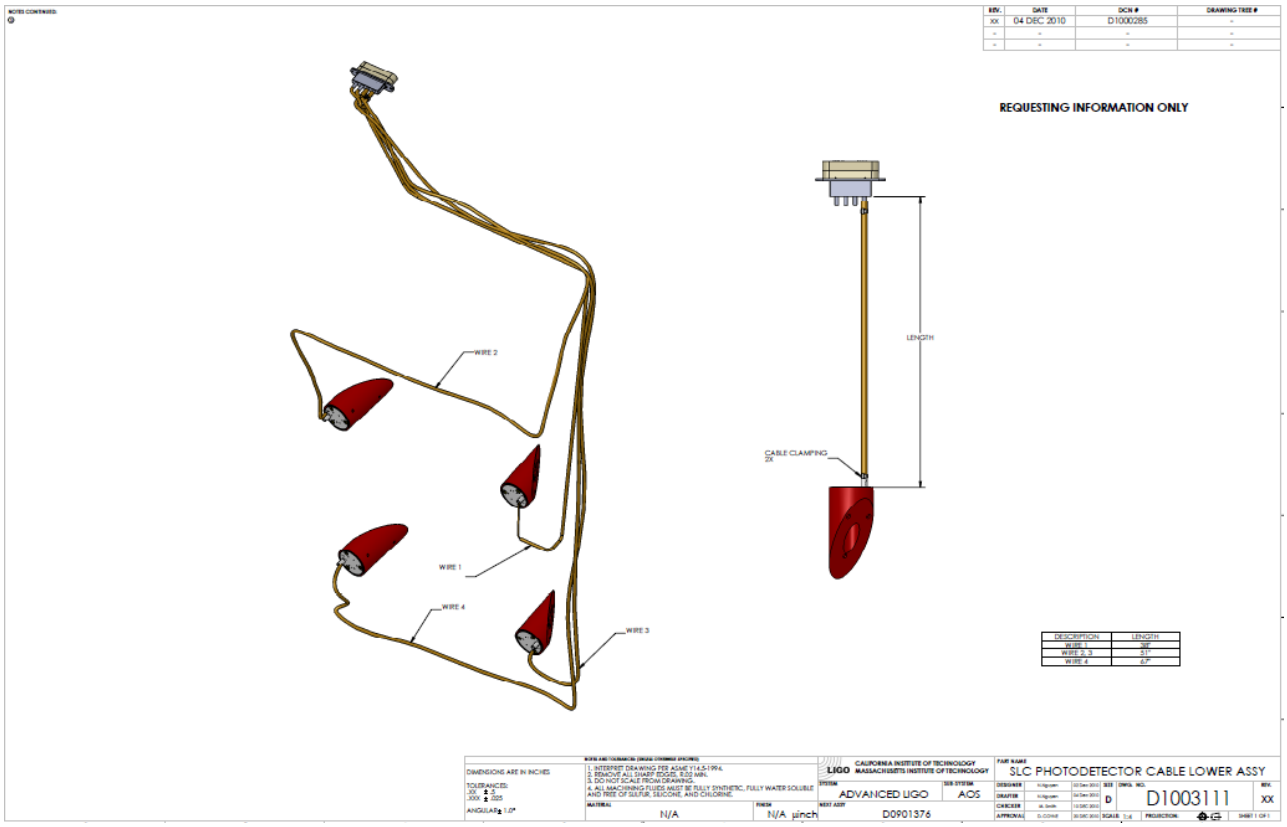

Figure 19: ALS Photo detector Cabling

Chamber	Cable length	Feedthrough
H1 BSC1	N/A	
H1 BSC3	N/A	
H1 BSC9	230"x2	LIGO-D1003081: Flange Layout – H1 Beam Splitter Chamber 9 (BSC9) ETMX
H1 BSC10	165"x2	LIGO-D1003082: Flange Layout – H1 Beam Splitter Chamber 10 (BSC10) ETMY
H2 BSC7	165"x2	LIGO-D1003086: Flange Layout – H2 Beam Splitter Chamber 7 (BSC7) ITMX
H2 BSC8	230"x2	LIGO-D1003087: Flange Layout – H2 Beam Splitter Chamber 8 (BSC8) ITMY
L1 BSC1	165"x1	LIGO-D1003088: Flange Layout – L1 Beam Splitter Chamber 1 (BSC1) ITMY
L1 BSC3	230"x1	LIGO-D1003090: Flange Layout – L1 Beam Splitter Chamber 3 (BSC3) ITMX
L1 BSC4	230"x1	LIGO-D1003091: Flange Layout – L1 Beam Splitter Chamber 4 (BSC4) ETMX
L1 BSC5	165"x1	LIGO-D1003092: Flange Layout – L1 Beam Splitter Chamber 5 (BSC5) ETMY

Number of Cable Clamps = ?

Number of 25D Cable Brackets = ?

3.5.1 Light Power on the ALS Photo detector

The ALS photo detectors are placed within the clear aperture of the Manifold/Cryopump Baffle and are visible from the opposite end of the arm beam tube, as shown in Figure 20.

When the IFO is in lock, each ALS photo detector will receive less than 1 microwatt from the wings of the 830000 W arm cavity beam; the dominant light flux will come from the scattered light from the opposite COC at the far end of the arm--this scattered light will illuminate each photo detector with approximately 4 E-3 W.

The ALS photodiodes will provide a diagnostic tool for monitoring the scattered light from the COC arm cavity mirrors.

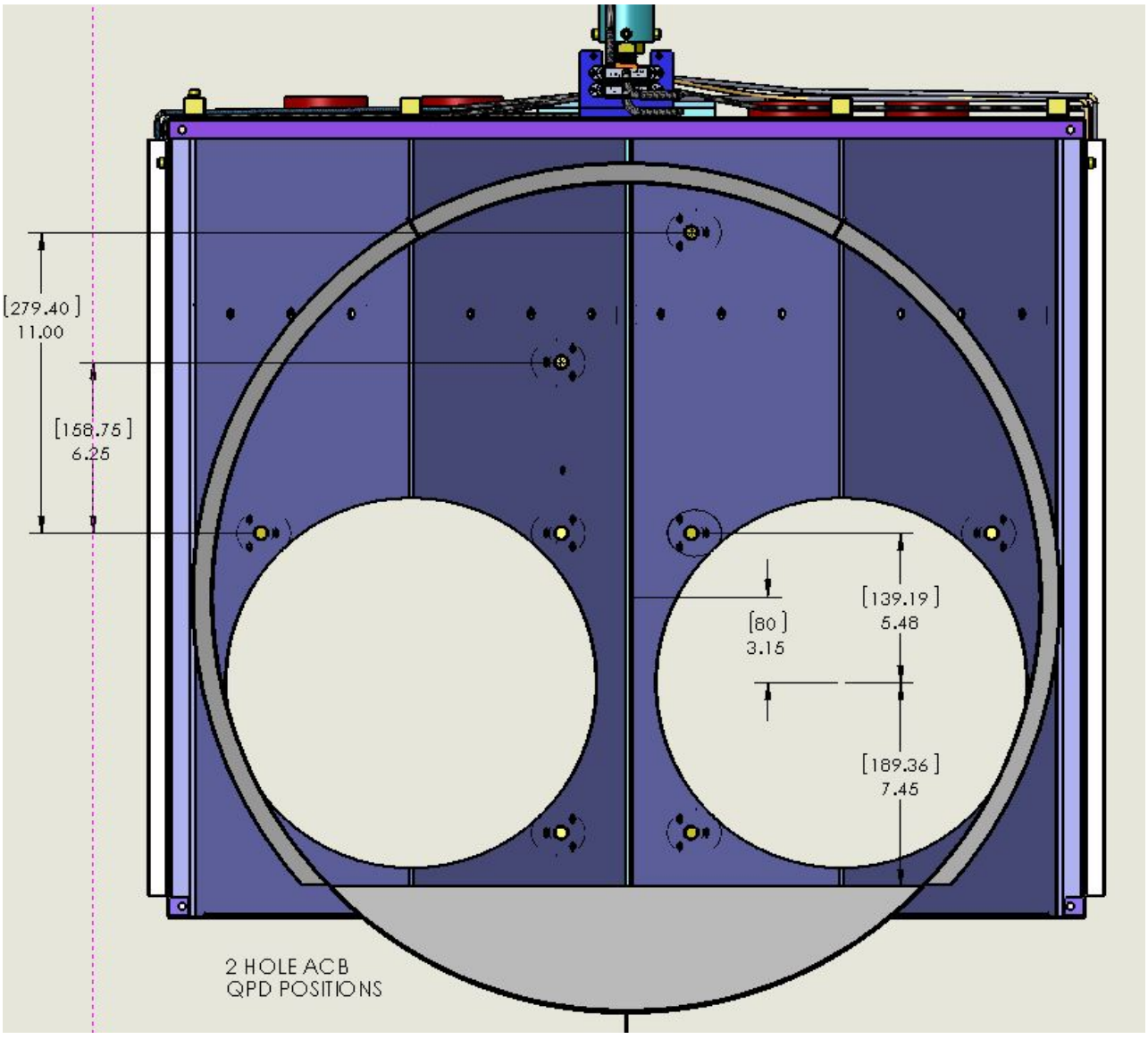

Figure 20: View toward the ALS Photo detector Array through the Manifold Cryopump Baffle Aperture

4 SCATTERED LIGHT DISPLACEMENT NOISE

The displacement noise caused by light scattering from the surface of the Arm Cavity Baffle, from the photo detector surface, and the surfaces of the fastening hardware is calculated in the following.

4.1 Arm Cavity Baffle Surface

The Arm Cavity Baffle Surface is black porcelainized steel, with a measured BRDF < 0.04E-2 sr^-1, as shown in

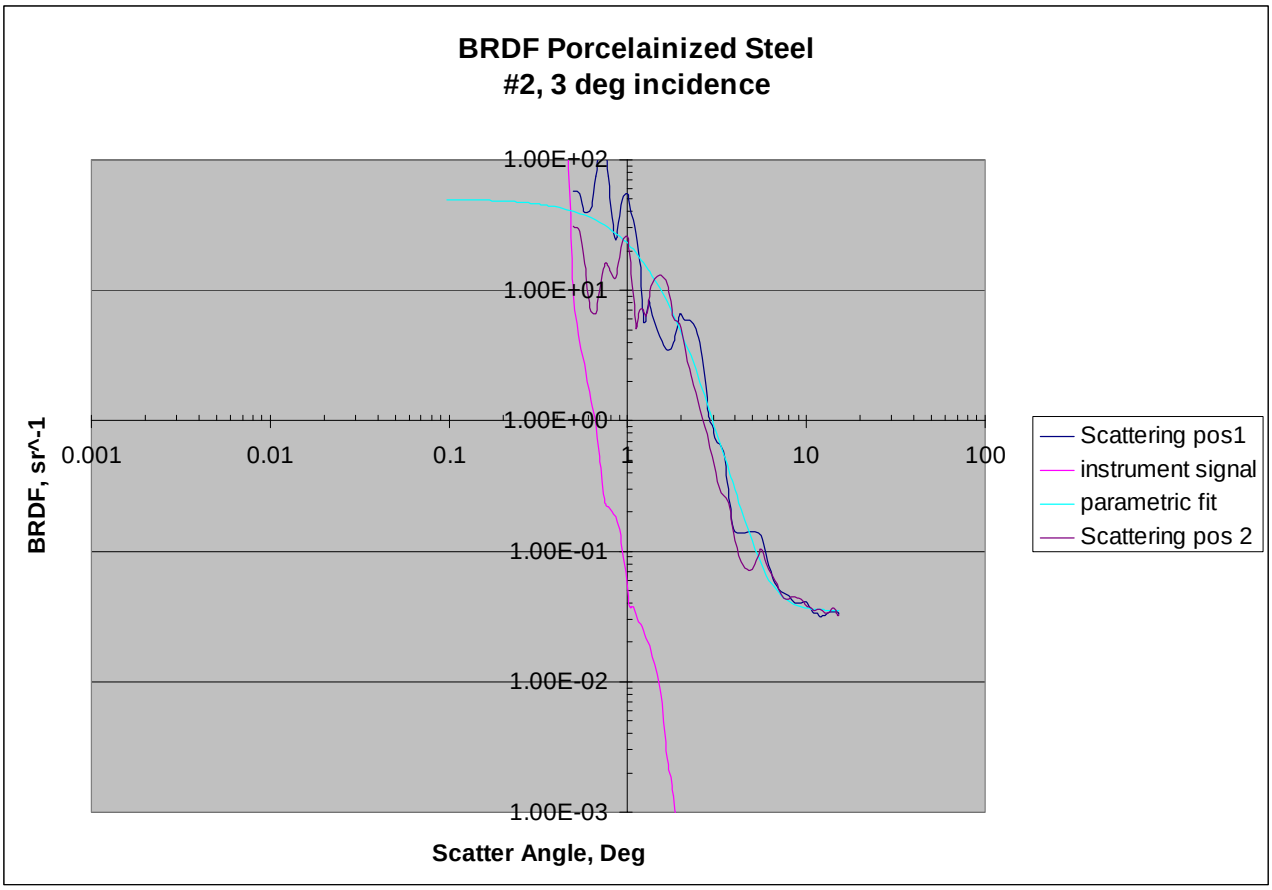

Figure 21: CASI Measurement of BRDF of Porcelainized Steel @ 3 Deg Incidence

The parametric equation with the best-fit to the scattering data is plotted in Figure 22.

$$BRDF_{ACB}(\theta_i) := \frac{BRDF_0}{\left(1 + C_{mr}\cdot\theta_i^{\,2}\right)^{\beta}} + BRDF_{\theta 2}$$

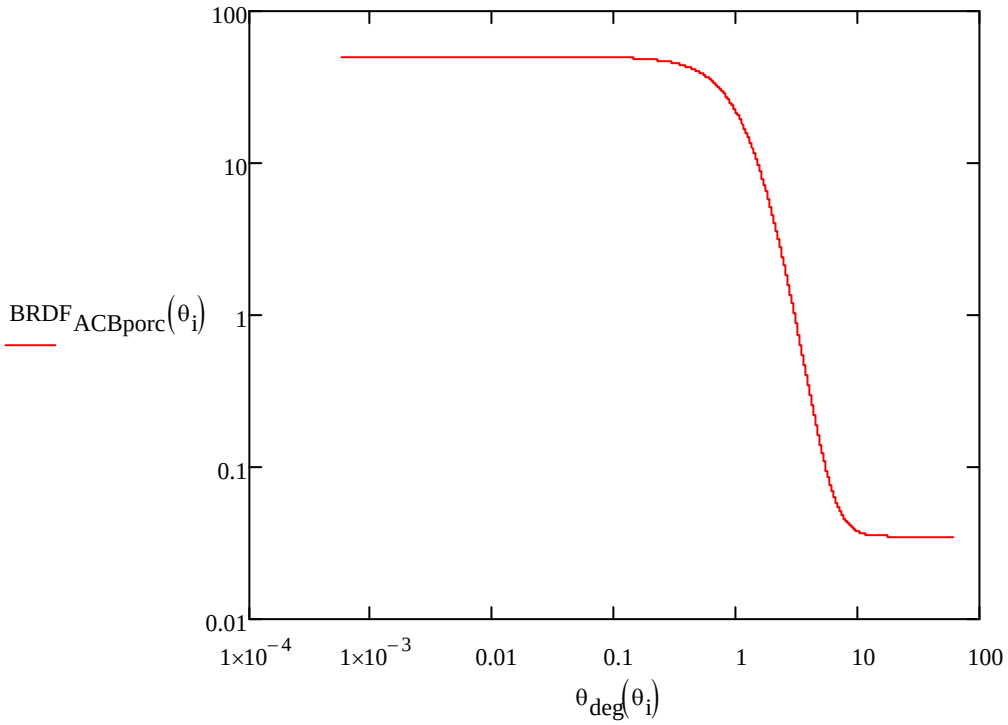

Figure 22: Parametric Equation, Porcelainized Steel BRDF Versus Scattering Angle Around the Specular Direction

4.1.1 Arm Cavity Baffle Surface Scatter

The primary source of scattered light from the Arm Cavity Baffle (ACB) is the small angle scatter from the COC mirror at the far end of the arm tube passes through the beam tube to the near arm cavity mirror. The power in the annulus between the cryopump baffle and the ITM (ETM) outside diameter will hit the Arm Cavity Baffle. See Figure 23. This light will scatter from the surface, and the edges and the bends of the ACB.

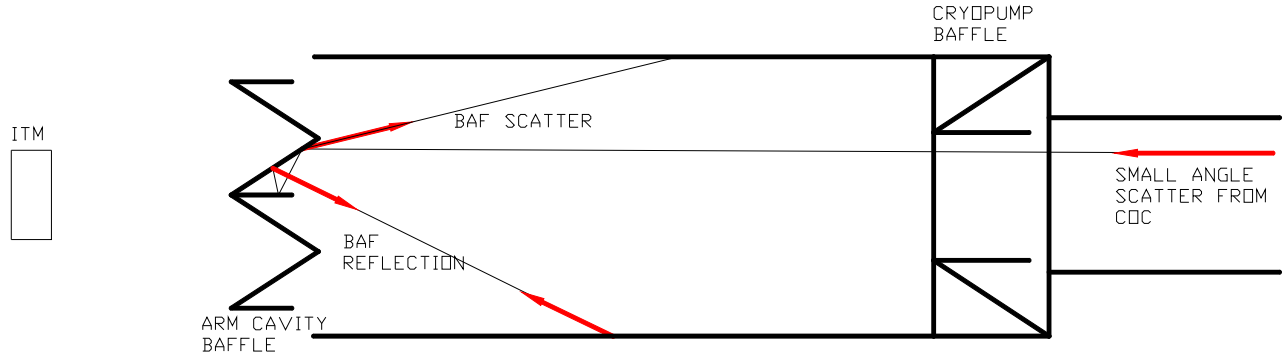

Figure 23: ARM CAVITY BAFFLE SCATTER

The scatter from the exposed frontal edges of the Arm Cavity Baffle depends upon the BRDF characteristics of the baffle material at small angles, upon the vertical tilt angle of the baffle edge, and upon the radius of the edge.

The scattering surface is suspended from the BSC ISI Stage 0 ring and has imposed on it the measured seismic motion in the beam direction, attenuated by the measured transmissibility of the Arm Cavity Baffle suspension. The motion spectrum of the Arm Cavity Baffle is shown in .

The details of the scattered light calculation are presented in T1100056. The results are presented below.

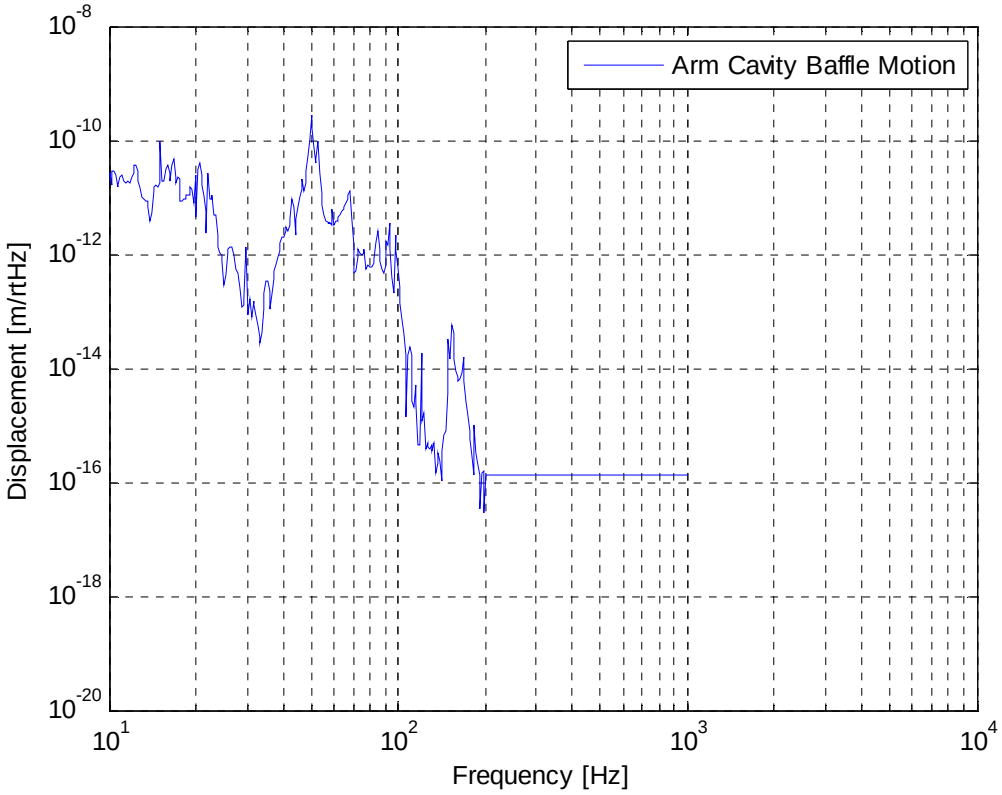

Figure 24: Motion Spectrum of ACB

The displacement noise @ 100 Hz due to the ACB scatter with an assumed baffle motion of 1E-12 m/rtHz, as a function of tilt angle, is shown in Figure 25.

$$DN_{acbporct}(\theta_t, r) := TF_{itmhr} \cdot \left(\frac{P_{acbporctsifo}(\theta_t, r)}{P_{psl}} \right)^{0.5} \cdot x_{ACB} \cdot 2 \cdot k$$

The measured BRDF of porcelainized steel at the 57 deg incident angle of the louver plates is

$$BRDF_{ACBporc}\left(2 \cdot 57 \cdot \frac{\pi}{180}\right) = 0.035$$

The glint portion of the displacement noise can be eliminated by tilting the ACB forward by 1 deg, so that the scattering from the louver surfaces dominates.

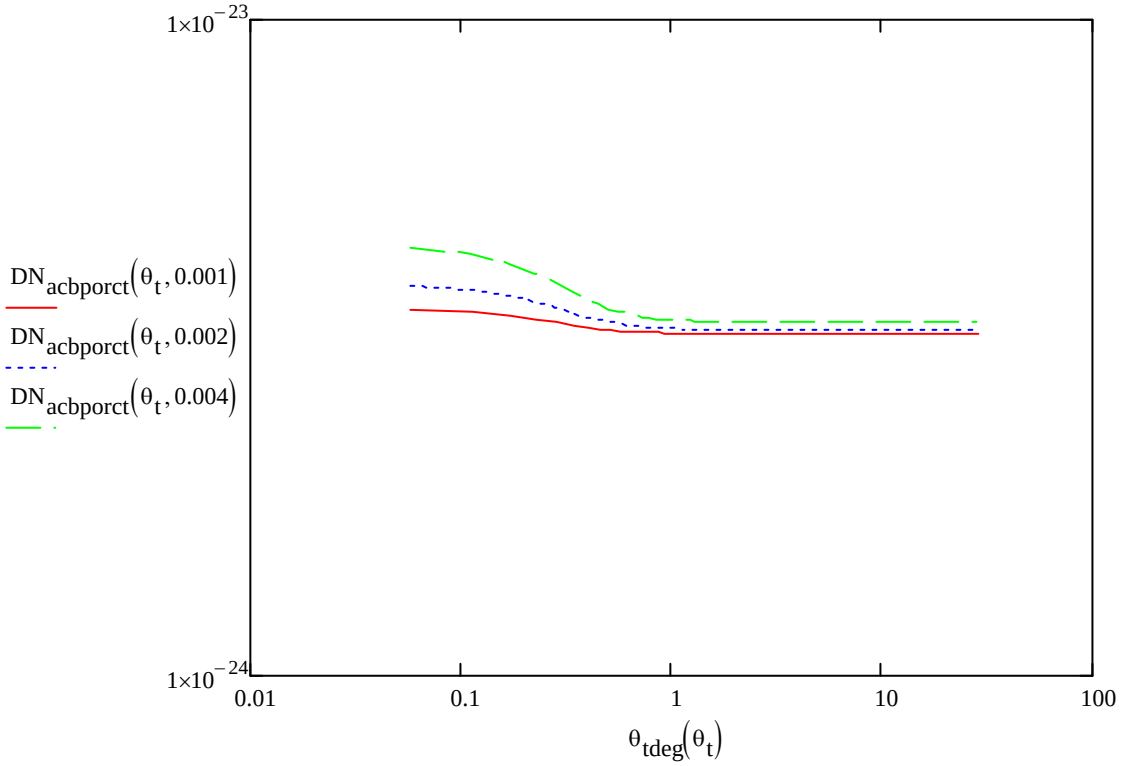

Figure 25: Displacement Noise, Total ACB Scatter, Porcelainized Steel

4.2 Scattered Light Displacement Noise from ALS Photo detector Array

The photo detector surfaces and the heads of the mounting screws will scatter the main beam and the COC scattered light beam from the far end of the beam tube. The displacement noise caused by these scattering sources is two orders of magnitude less than that of the Arm Cavity Baffle surface.

4.3 Scattered Light Calculation Parameters

laser wavelength, m

$$\lambda := 1.064 \cdot 10^{-6}$$

wave number, m^-1

$$k := 2 \cdot \frac{\pi}{\lambda}$$

$$k = 5.9052 \times 10^{6}$$

IFO waist size, m

$$w_{ifo} := 0.012$$

solid angle of IFO mode, sr

$$\Delta_{ifo} := \frac{\lambda^2}{\pi \cdot w_{ifo}^2}$$

$$\Delta_{ifo} = 2.5025 \times 10^{-9}$$

Transfer function @ 100 Hz, ITM HR

$$TF_{itmhr} := 1.1 \cdot 10^{-9}$$

Gaussian beam radius at ITM, m

$$w := 0.055$$

IFO arm length, m

$$L := 4000$$

PSL laser power, W

$$P_{psl} := 125$$

Arm Power, W

$$P_0 := 834174$$

BRDF, sr^-1; CSIRO, surface 2, S/N 2

$$BRDF_1(\theta) := \frac{2755.12}{\left(1 + 8.50787 \cdot 10^{8} \cdot \theta^2\right)^{1.23597}}$$

BRDF_porcelain_ss

$$BRDF_{porc} := 2 \cdot 10^{-3}$$

BRDF of photo detector, sr^-1

$$BRDF_{pd} := 1 \cdot 10^{-3}$$

BRDF of screw head sr^-1

$$BRDF_{sh} := 5 \cdot 10^{-2}$$

BRDF_COC_30urad, sr^-1

$$BRDF_{COC} := BRDF_1\left(30 \cdot 10^{-6}\right)$$

$$BRDF_{COC} = 1.3644 \times 10^{3}$$

number of photo detector $N_{pd} := 16$

number of screw heads $N_{sh} := 48$

radius of photo detector ring, m $r_{pdbc} := 0.196$

Photoconductor radius, m $r_{pd} = 5.7 \times 10^{-3}$

photoconductor area, m^2 $A_{pd} := \pi \cdot r_{pd}^{2}$ $A_{pd} = 1.0207 \times 10^{-4}$

Screw head radius, m $r_{sh} := .0038$

Screw head area, m^2 $A_{sh} := \pi \cdot r_{sh}^{2}$ $A_{sh} = 4.5365 \times 10^{-5}$

4.4 Scattering of Main Arm Beam

4.4.1 Power Hitting Photo detector Surface and Screw Head

irradiance function at ACB, W/m^2 $I_{pd}(r) := 2 \cdot \frac{P_0}{\pi \cdot w^2} \cdot e^{-2 \cdot \left(\frac{r^2}{w^2}\right)}$

total beam power, W $P_0 := \int_0^{10w} 2 \cdot \pi \cdot r \cdot I_{pd}(r)\, dr$

$P_0 = 8.3417 \times 10^{5}$

Irradiance at photo detector, W/m^2 $I_{pd}(r_{pdbc}) = 1.6359 \times 10^{-3}$

$P_{pd} := I_{pd}(r_{pdbc}) \cdot A_{pd}$

Power hitting each PD, W

$$P_{pd} = 1.6698\times 10^{-7}$$

Power hitting each screw head, W

$$P_{sh} := I_{pd}\left(r_{pdbc}\right)\cdot A_{sh}$$

$$P_{sh} = 7.4213\times 10^{-8}$$

4.4.2 Power Scattered into IFO Mode

half-angle from centerline to inner edge of PD, rad

$$\theta_{pdi} := \frac{\left(r_{pdbc} - r_{pd}\right)}{L}$$

half-angle from centerline to outer edge of PD, rad

$$\theta_{pdo} := \frac{\left(r_{pdbc} + r_{pd}\right)}{L}$$

average angle, rad

$$\theta_{pd} := \frac{\theta_{pdi} + \theta_{pdo}}{2}$$

$$\theta_{pd} = 4.9\times 10^{-5}$$

BRDF at photo detector, angle, sr^-1

$$BRDF_1\left(4.9\times 10^{-5}\right) = 696.3695$$

4.4.2.1 Scattering by Photo detector

power scattered by photo detector, into IFO mode, W

$$P_{pds} := \sqrt{N_{pd}}\cdot P_{pd}\cdot BRDF_{pd}\cdot\frac{\pi\cdot w_{ifo}^{2}}{L^{2}}\cdot BRDF_1\left(4.9\times 10^{-5}\right)\cdot\Delta_{ifo}$$

$$P_{pds} = 3.291\times 10^{-26}$$

4.4.2.2 Scattering by Screw Head

power scattered by screw head into IFO mode, W

$$P_{shs} := \sqrt{N_{sh}} \cdot P_{sh} \cdot BRDF_{sh} \cdot \frac{\pi \cdot w_{ifo}^{2}}{L^{2}} \cdot BRDF_{1}\left(4.9 \times 10^{-5}\right) \cdot \Delta_{ifo}$$

$$P_{shs} = 1.2667 \times 10^{-24}$$

4.4.3 Displacement Noise

ACB displacement @ 100 HZ, m/rt HZ $x_{ACB} := 1 \cdot 10^{-12}$

displacement noise @ 100 Hz, m/rtHz $DN_{acbpd} := TF_{itmhr} \cdot \left(\frac{P_{pds}}{P_{psl}}\right)^{0.5} \cdot x_{ACB} \cdot 2 \cdot k$

$$DN_{acbpd} = 2.108 \times 10^{-28}$$

4.5 Scattering from COC Scattered Stray Light

4.5.1 Power Hitting Photo detector Surface and Screw Head

COC Scattered power hitting the PD, W $P_{cocpd} := P_0 \cdot BRDF_1\left(\theta_{pd}\right) \cdot \frac{A_{pd}}{L^{2}} = 3.7057 \times 10^{-3}$

COC Scattered power hitting the screw head W $P_{cocsh} := P_0 \cdot BRDF_1\left(\theta_{pd}\right) \cdot \frac{A_{sh}}{L^{2}} = 1.647 \times 10^{-3}$

4.5.2 Power Scattered into IFO Mode

4.5.2.1 Scattering by Photo detector

power scattered by photo detector,
into IFO mode, W

$$P_{cocpds} := \sqrt{N_{pd}} \cdot P_{cocpd} \cdot BRDF_{pd} \cdot \frac{\pi \cdot w_{ifo}^{2}}{L^{2}} \cdot BRDF_1\left(4.9 \times 10^{-5}\right) \cdot \Delta_{ifo}$$

$$P_{cocpds} = 7.3036 \times 10^{-22}$$

4.5.2.2 Scattering by Screw Head

power scattered by screw head
into IFO mode, W

$$P_{cocshs} := \sqrt{N_{sh}} \cdot P_{cocsh} \cdot BRDF_{sh} \cdot \frac{\pi \cdot w_{ifo}^{2}}{L^{2}} \cdot BRDF_1\left(4.9 \times 10^{-5}\right) \cdot \Delta_{ifo}$$

$$P_{cocshs} = 2.8112 \times 10^{-20}$$

4.5.3 Displacement Noise

displacement noise @ 100 Hz, m/rtHz

$$DN_{cocpd} := TF_{itmhr} \cdot \left(\frac{P_{cocpds}}{P_{psl}}\right)^{0.5} \cdot x_{ACB} \cdot 2 \cdot k$$

$$DN_{cocpd} = 3.1403 \times 10^{-26}$$

$$DN_{cocsh} := TF_{itmhr} \cdot \left(\frac{P_{cocshs}}{P_{psl}}\right)^{0.5} \cdot x_{ACB} \cdot 2 \cdot k$$

$$DN_{cocsh} = 1.9483 \times 10^{-25}$$

4.6 Scattering from COC Scattered Light that Passes through the Optlev Hole in FETM ACB

4.6.1 Power Passing through Optlev Hole that Hits the Transmon Telescope Housing

projected minor radius of optlev opening in ACB, m $R_{minoptlev} := .020$

projected major radius of optlev opening in ACB, m $R_{majoptlev} := 0.27$

projected area of optlev opening in ACB, m^2 $A_{optlev} := 0.6 \cdot \left(\pi \cdot R_{minoptlev} \cdot R_{majoptlev}\right)$

$A_{optlev} = 0.01$

The intensity of light scattered from the ITM HR surface that is incident on the optlev hole and the power that passes through the hole is given by the following:

incident intensity, W/m^2 $I_i := \frac{P_{acb}}{A_{cp}} = 31.376$

power passing through ACB optlev hole, W $P_{optlev} := I_i \cdot A_{optlev}$

$P_{optlev} = 0.319$

4.6.2 Power Scattered into IFO Mode

The surface of the TMS telescope housing is machined aluminum. It is aligned with an angle of incidence nearly normal to the stray light beam. We will assume that the BRDF at normal incidence is approximately 1.0 sr^-1; by comparison, the BRDF of oxidized polished stainless steel at normal incidence is on the order of 10 sr^-1.

estimated BRDF of TMS frame @ near normal incidence, sr^-1 $BRDF_{TMSframe} := 1$

The power scattered into the IFO mode is given by the following:

power scattered by TMS optlev hole into IFO, W

$$P_{TMSframesifo} := P_{optlev} \cdot BRDF_{TMSframe} \cdot \frac{w_{ifo}^{2}}{L_{arm}^{2}} \cdot BRDF_1\left(30 \cdot 10^{-6}\right) \cdot \Delta\Omega_{ifo}$$

$P_{TMSframesifo} = 9.814 \times 10^{-18}$

4.6.3 Displacement Noise

The motion of the TMS frame is required to be less than 2E-12 m/rtHz, according to G0900293 Transmon Sensitivity Calculations.

motion of TMS frame
see G0900293, m/rt Hz

$$x_{TMS} := 2 \cdot 10^{-12}$$

The stray light is scattered directly into the IFO mode via the ITM mirror HR surface, and the scattered light displacement noise at 100 Hz is given below:

displacement noise @ 100 Hz, m/rtHz

$$DN_{TMSoptlev} := TF_{itmhr} \cdot \left(\frac{P_{TMSframesifo}}{P_{psl}} \right)^{0.5} \cdot x_{TMS} \cdot 2 \cdot k$$

$$DN_{TMSoptlev} = 7.281 \times 10^{-24}$$

4.7 Total Displacement Noise from Arm Cavity Beam and COC Scattered Stray Light

The full scattering displacement noise spectrum from the Arm Cavity Beam and the COC scattered stray light is shown in Figure 26, and is compared with the AOS requirement.

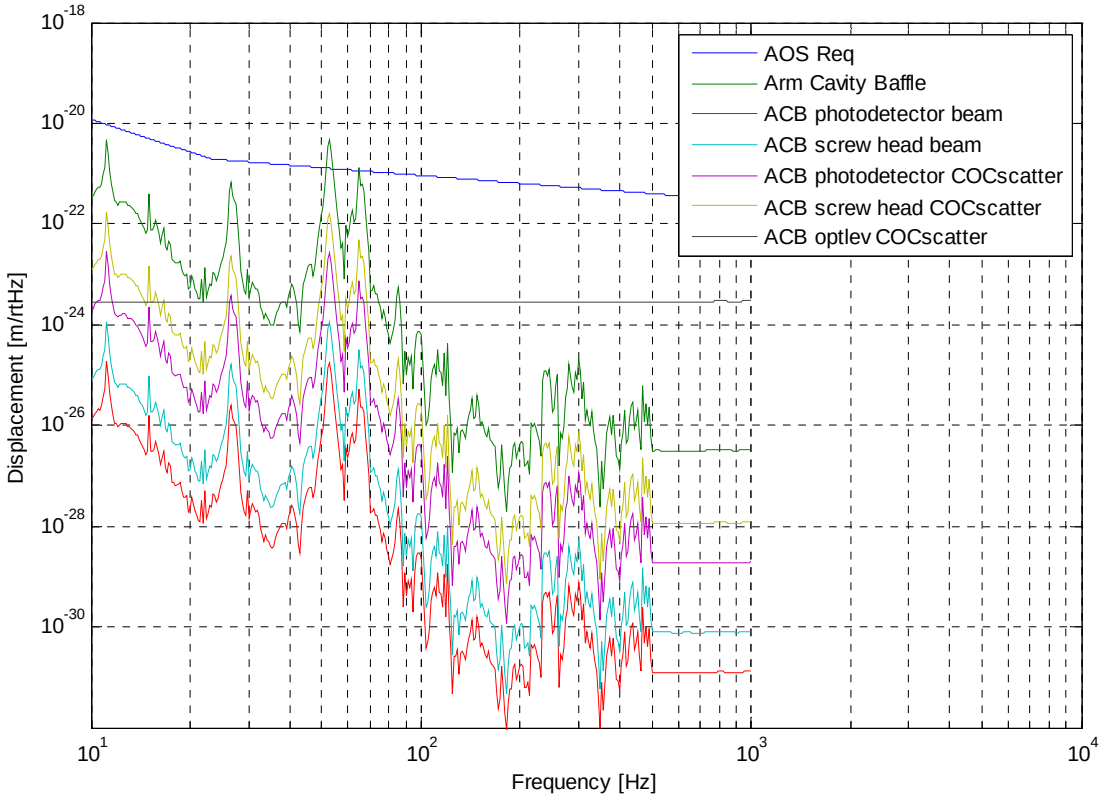

Figure 26: Scattered Light Displacement Noise from Arm Cavity Beam, and from the COC Scattered Stray Light

4.8 Wide Angle Scattering from ITM TM

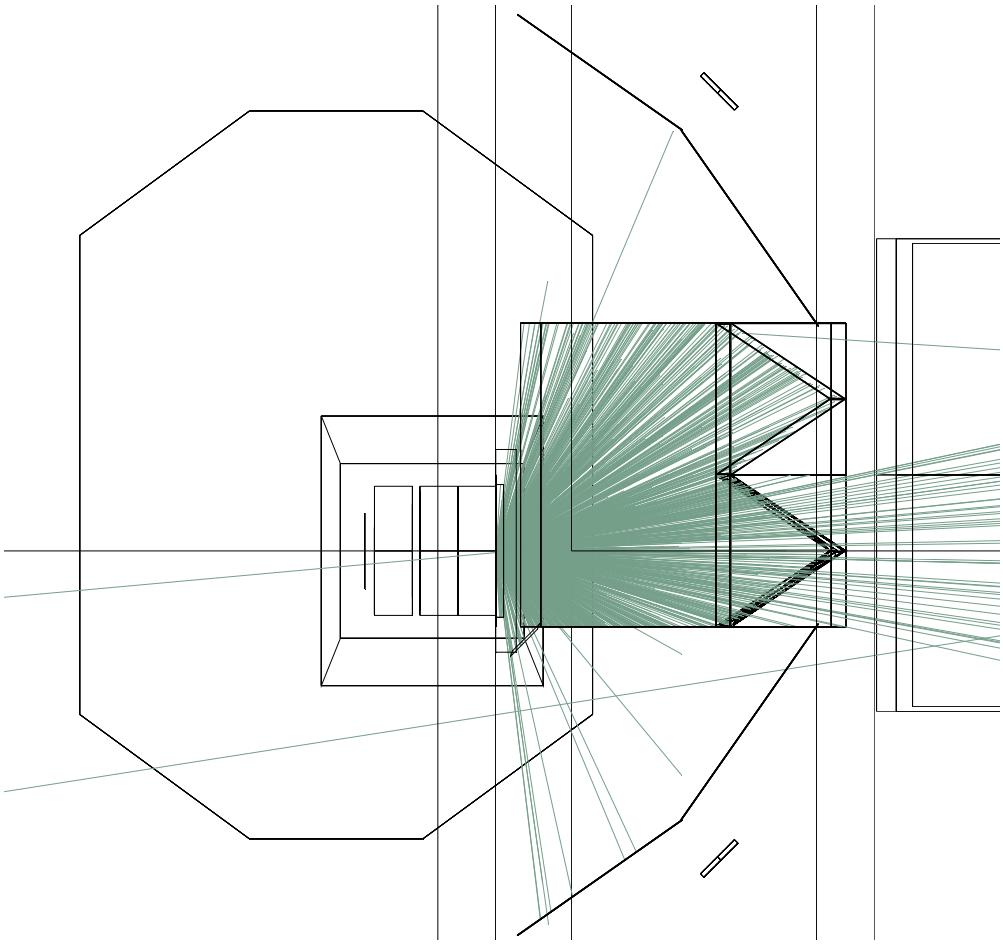

Figure 27: ZEMAX Lambertian Scatter Ray Trace from H1 ITMX HR, Top View

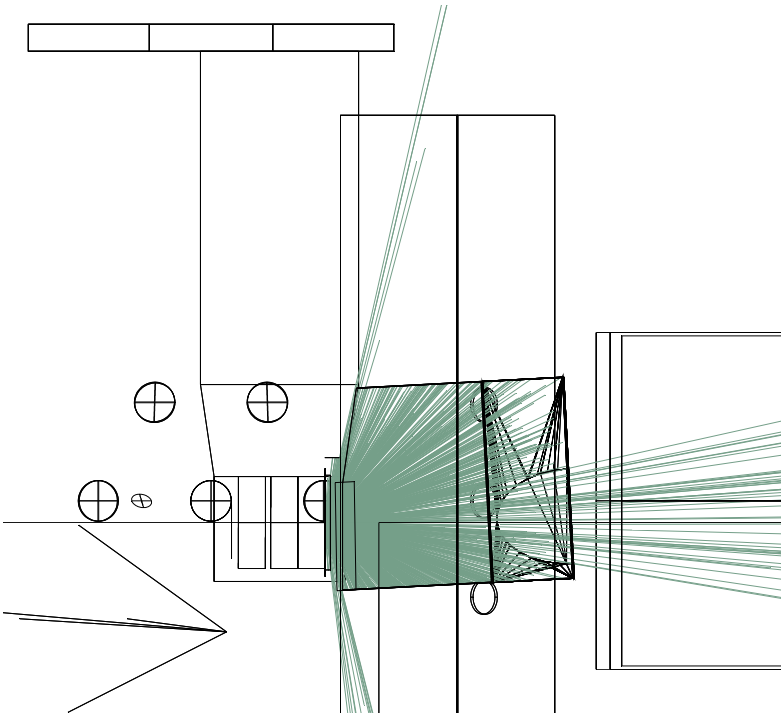

Figure 28: ZEMAX Lambertian Scatter Ray Trace from H1 ITMX HR, ACB with Wide Angle Baffle Sides, side view

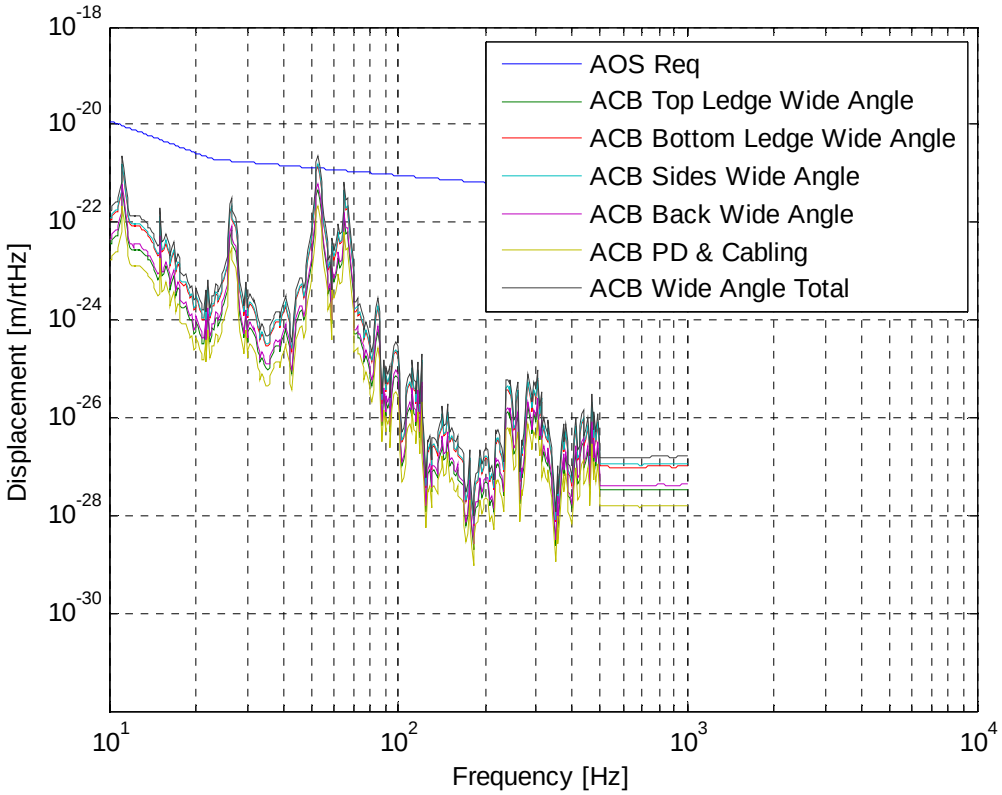

Figure 29: TM Wide Angle Displacement Noise from Various Parts of the ACB

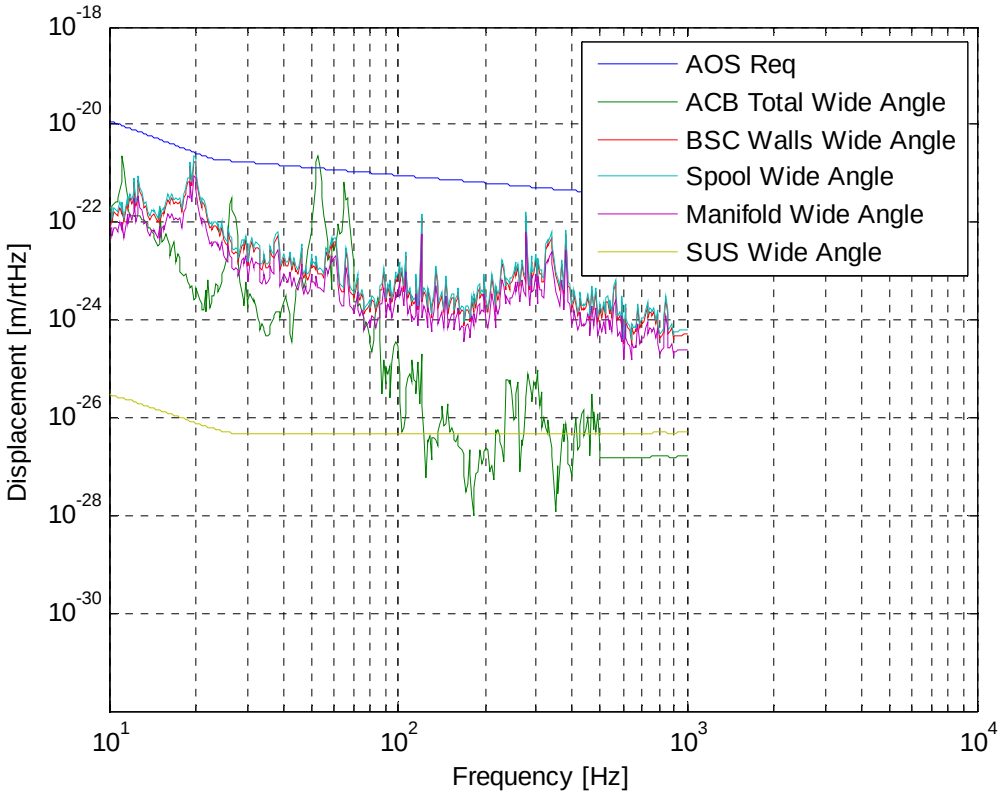

Figure 30: Total Components of TM Wide Angle Scattering

4.9 Wide Angle Scattering from ETM TM

Lambertian scattering from the ETM mirror was modeled in ZEMAX, and a ray trace of the scattered light is shown in the following figures.

More than 75% of the wide-angle scattered light is captured by the ACB and wide angle box. 4% passes through the hole in the arm cavity baffle and hits the 7A2 spool piece or the support structure for the Photon Calibrator mirrors.

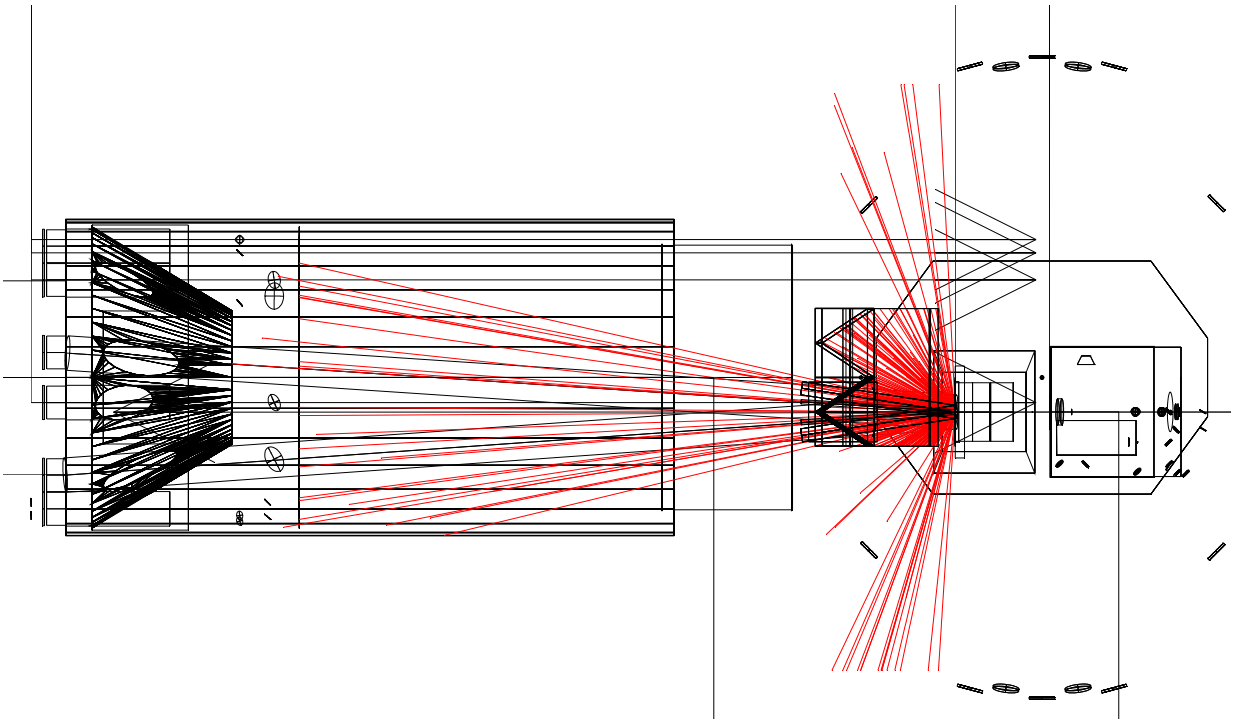

Figure 31: ZEMAX Lambertian Scatter Ray Trace from H1 ETMX HR, Top View

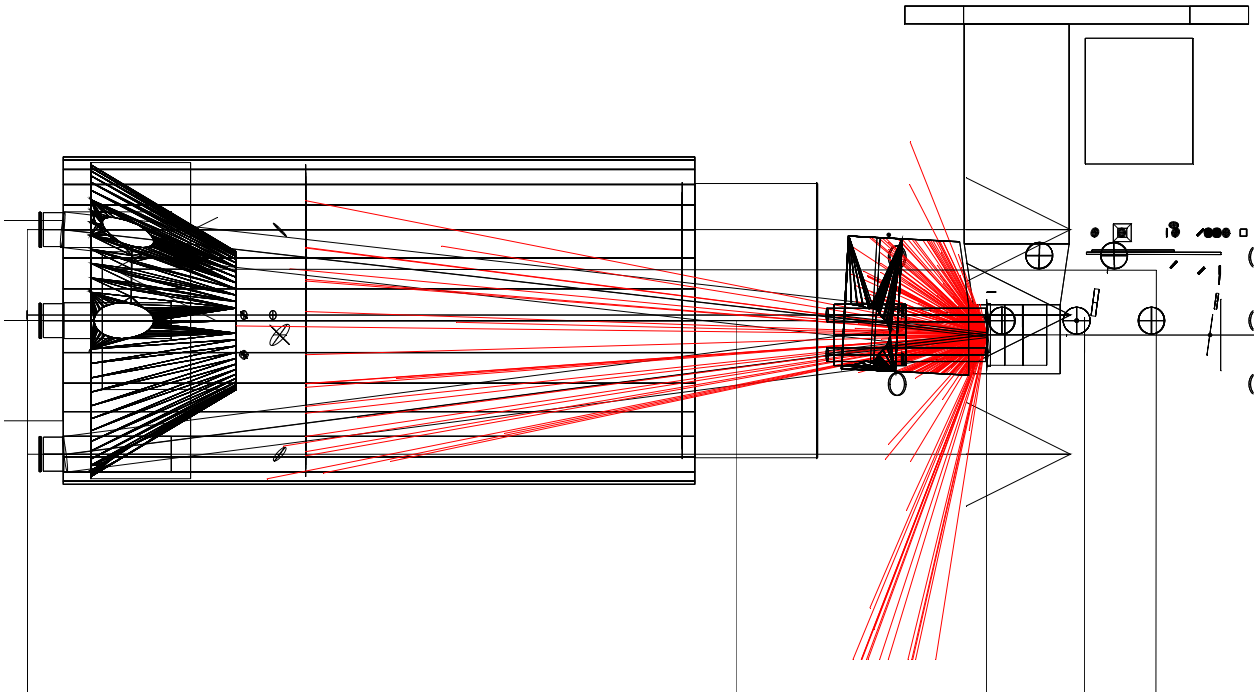

Figure 32: ZEMAX Lambertian Scatter Ray Trace from H1 ITMX HR, ACB with Wide Angle Baffle Sides, side view

fractional power hitting PCal structure, W $PF_{PCal} := 0.027$

incident power hitting PCal structure, W $P_{PCal} := P_a \cdot PF_{PCal} \cdot \alpha_L$ $P_{PCal} = 0.226$

4.9.1 Wide Angle Scattering from Photon Calibrator Support Structure

The surface of the PCal support structure is machined aluminum. We will assume that the BRDF at is approximately the same as the rough spool piece wall, 0.1 sr^-1.

angle from PCal structure, rad $\theta_{PCal} := 0.0$

distance from PCal structure, m $L_{PCal} := 2.37$

wide angle hemispherical scattering loss fraction from TM wide, ref: T070089 $\alpha_L := 10 \times 10^{-6}$

BRDF of chamber wall, sr^-1 $BRDF_{wall} := 0.1$

The power scattered into the IFO mode is given by the following:

PCal structure, W

$$P_{PCalifo} := \sqrt{4} \cdot P_{PCal} \cdot \left(\frac{\lambda^2}{L_{PCal}^2} \cdot BRDF_{wall} \cdot \alpha_L \cdot \frac{\left|\cos\left(\theta_{PCal}\right)\right|}{\pi} \right)$$

$P_{PCalifo} = 2.884 \times 10^{-20}$

4.9.2 Displacement Noise

Motion of manifold @ 100 Hz, m/rt Hz $x_{manifold} := 8 \cdot 10^{-11}$

The stray light is re-scattered from the Lambertian surface of the ETM directly into the IFO mode, and the scattered light displacement noise at 100 Hz is given below:

PCal structure

$$DN_{PCal} := TF_{itmhr} \cdot \left(\frac{P_{PCalifo}}{P_{psl}} \right)^{0.5} \cdot x_{manifold} \cdot 2 \cdot \frac{k}{\sqrt{2}}$$

$$DN_{PCal} = 1.116 \times 10^{-23}$$

Displacement Noise Requirement @ 100 Hz, m/rt Hz $D_{req} = 1 \times 10^{-21}$

5 INTERFACES

5.1 Installation of the Arm Cavity Baffle in the BSC Chamber

Update the doc with E1100810

The suspension assembly for the Arm Cavity Baffle will be installed on ISI Stage 0 while it is on the Cartridge prior to insertion into the BSC Chamber, as shown in Figure 33.

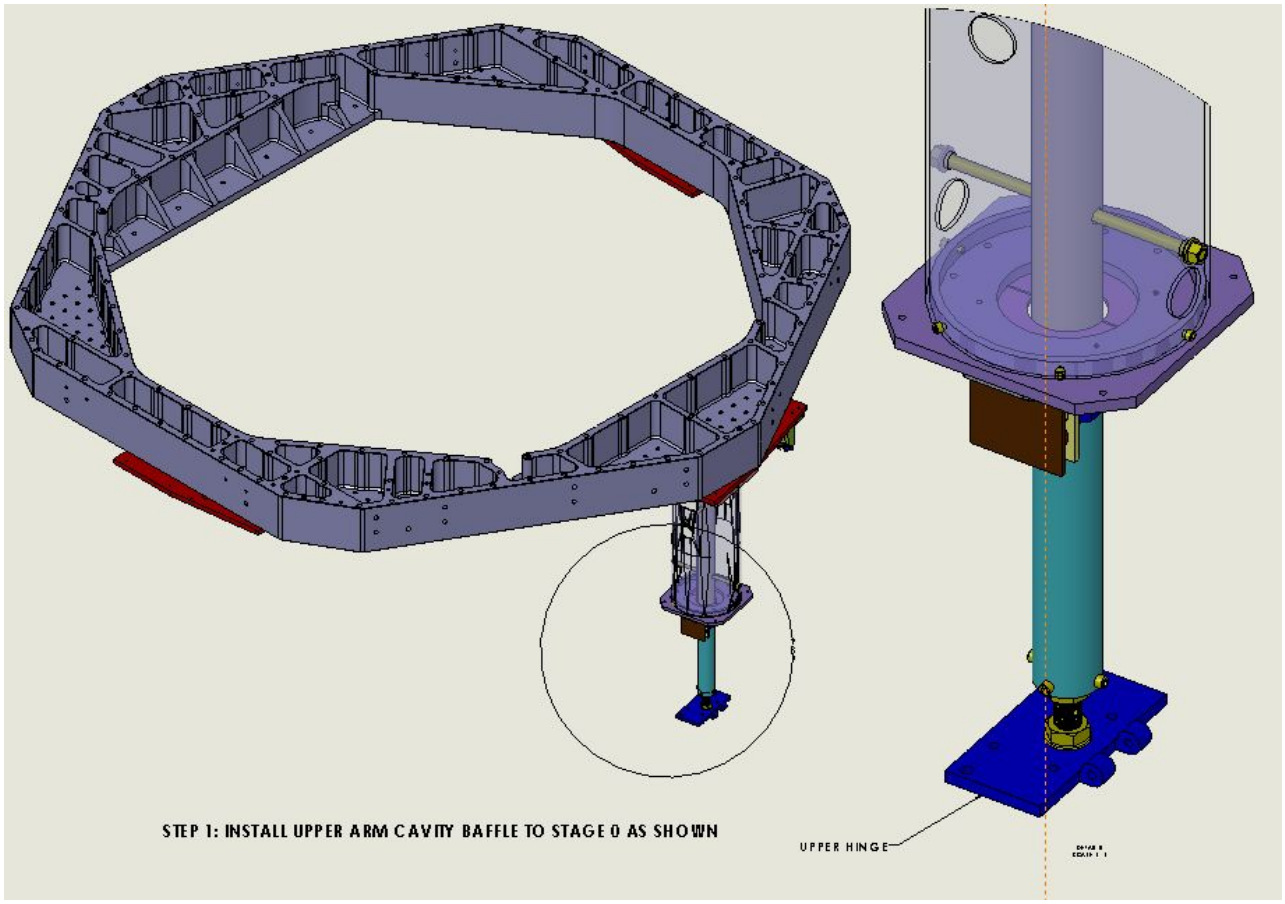

Figure 33: Installation of Arm Cavity Baffle Suspension Assembly while in the Cartridge

Once the ISI Stage 0 has been inserted into the BSC chamber, and after the Quad Suspensions have been installed, the lower portion of the Arm Cavity Baffle will be brought into the BSC chamber and attached to the upper hinge, as shown in

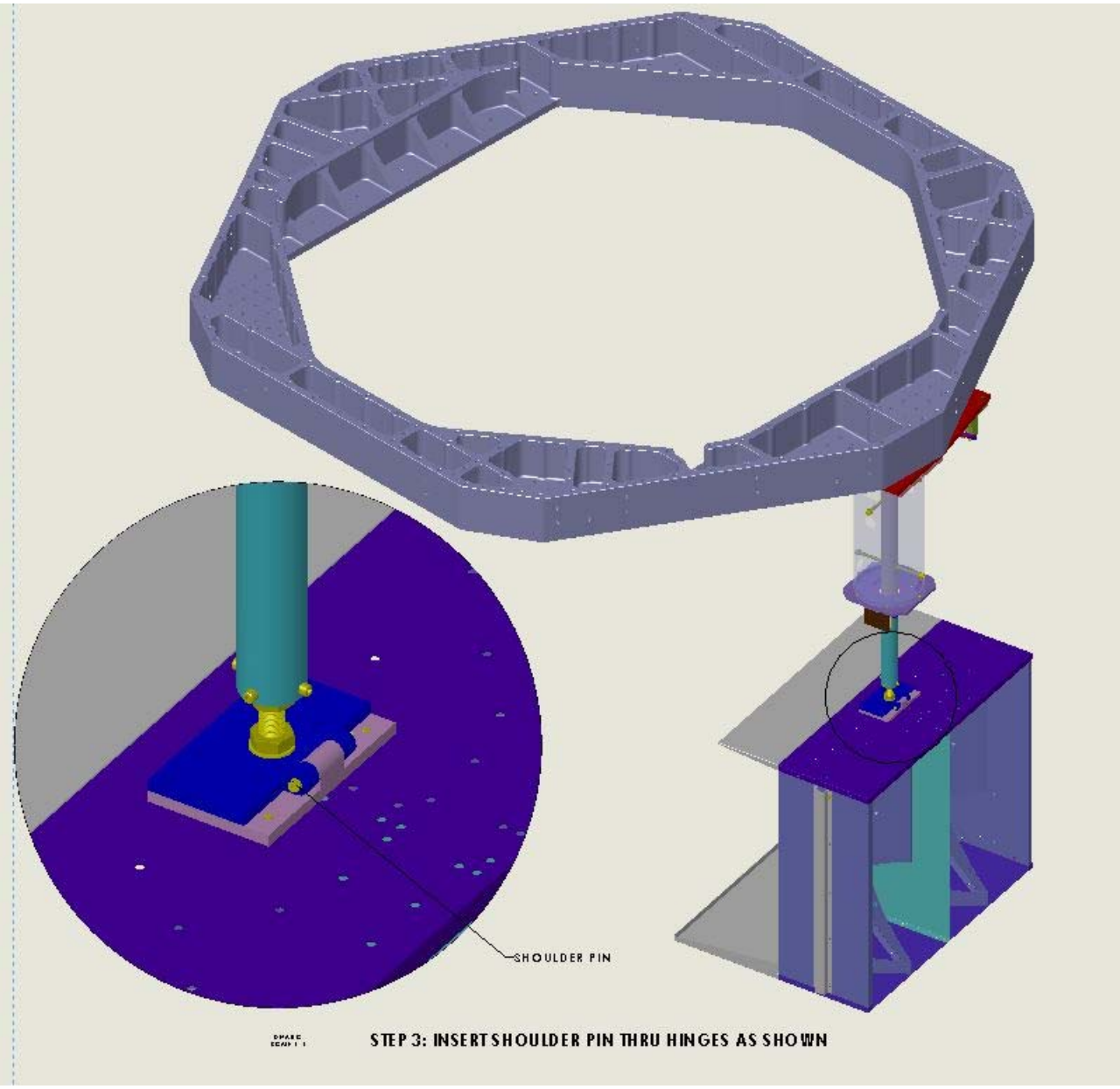

Figure 34: Attachment of Lower Arm Cavity Baffle Assembly to the Suspension

5.2 Interface to ITM and ETM Mirrors

The Arm Cavity Baffle meets the requirement of giving access to the ITM and ETM mirrors and suspension by being hinged out of the way, as described in 3.3. The distance between the wide angle baffle box and the quad suspension frame before hinging away will be set to 2.0 inches.

Table 5: ACB Distance from TM

CHAMBER	Arm Cavity Baffle Distance, inches	Comments
BSC1-H1	18.13	
BSC3-H1	23.70	
BSC9-H1	18.01	Support tubes are parallel to ACB
BSC10-H1	18.05	Support tubes are parallel to ACB
BSC5-H2	17.0	Support tubes are parallel to ACB
BSC6-H2	17.1	Support tubes are parallel to ACB
BSC7-H2	16.17	Support tubes are parallel to ACB
BSC8-H2	17.07	Support tubes are parallel to ACB

5.3 Interface to ISI Stage 0

The Arm Cavity Baffle suspension support plate is attached to the ISI Stage 0 by means of clamps fastened with bolts into the threaded holes of the Stage 0. The locations of the support plate on the ISI Stage 0 for the various BSC chambers is shown in Figure 35.

One lesson learned from the Arm Cavity Baffle suspension test at LASTI is that the support plate should be clamped as close as possible to the down tube of the suspension structure to avoid resonances due to cantilever flexing of the support plate.

A Solid Works drawing of the Arm Cavity Baffle in its installed position in BSC 8 is shown in Figure 43.

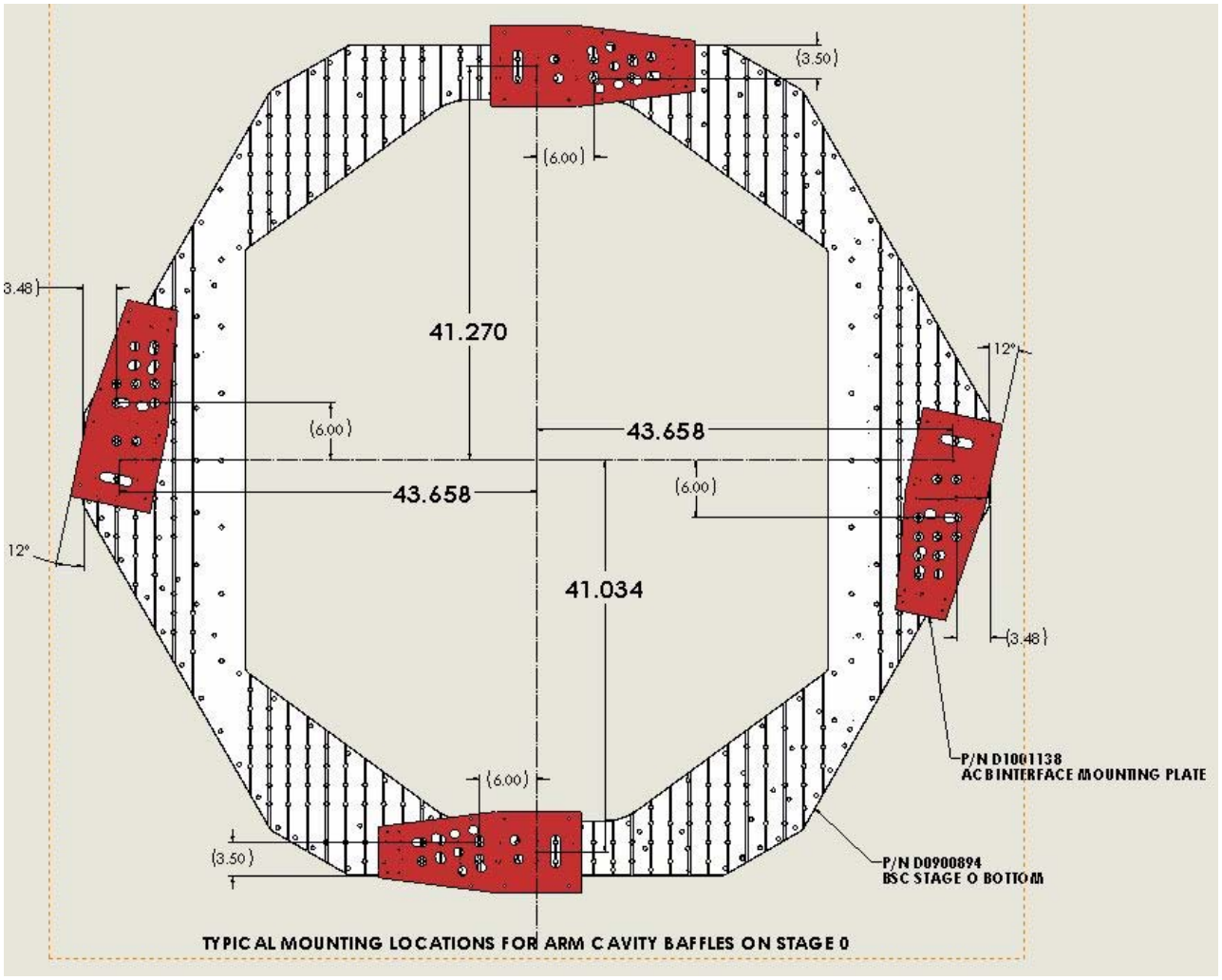

Figure 35: Mounting locations of the Arm Cavity Baffle in the Various BSC Chambers.

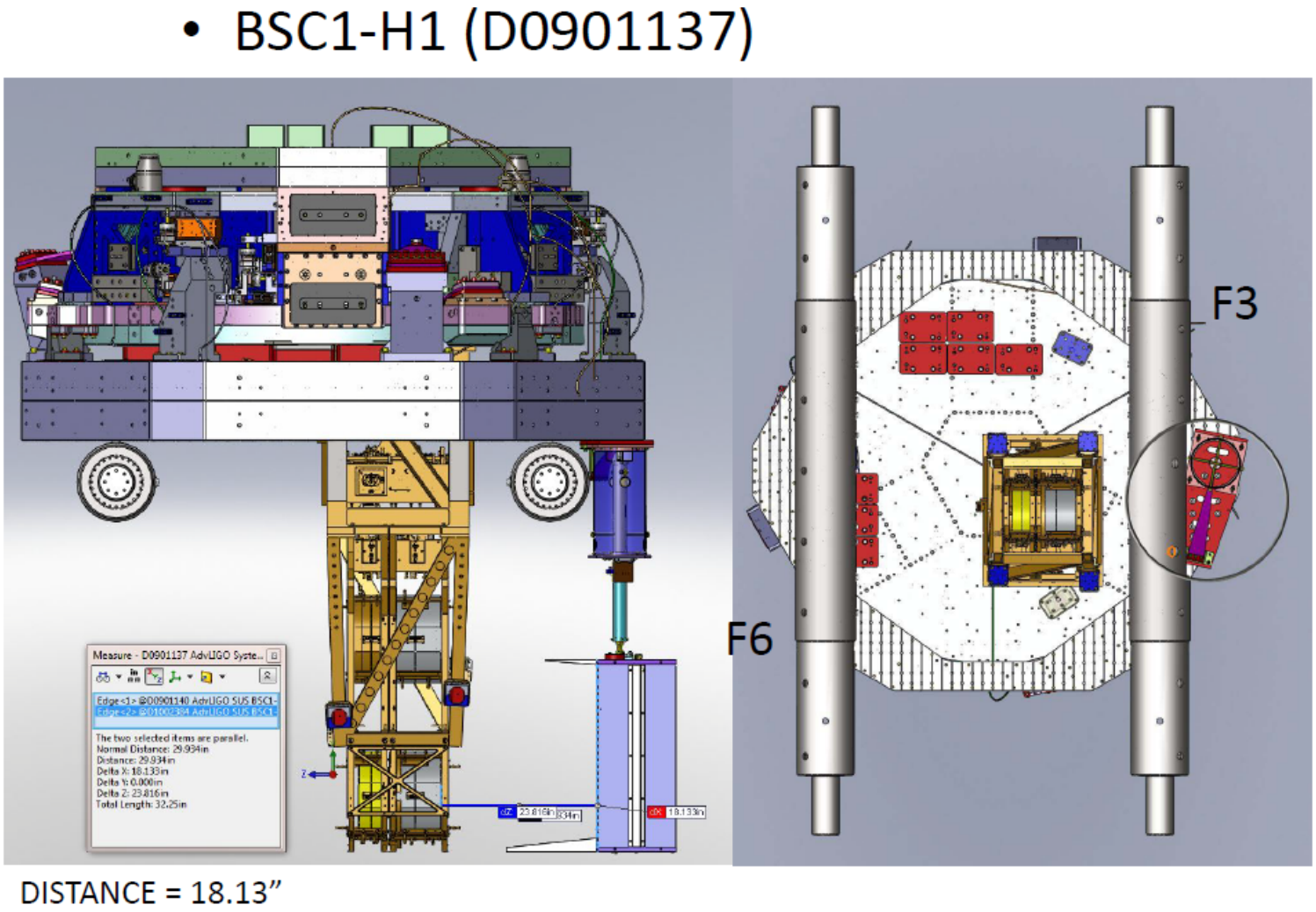

Figure 36: Arm Cavity Baffle Installed in BSC1-H1

- BSC3-H1 (D0901146)

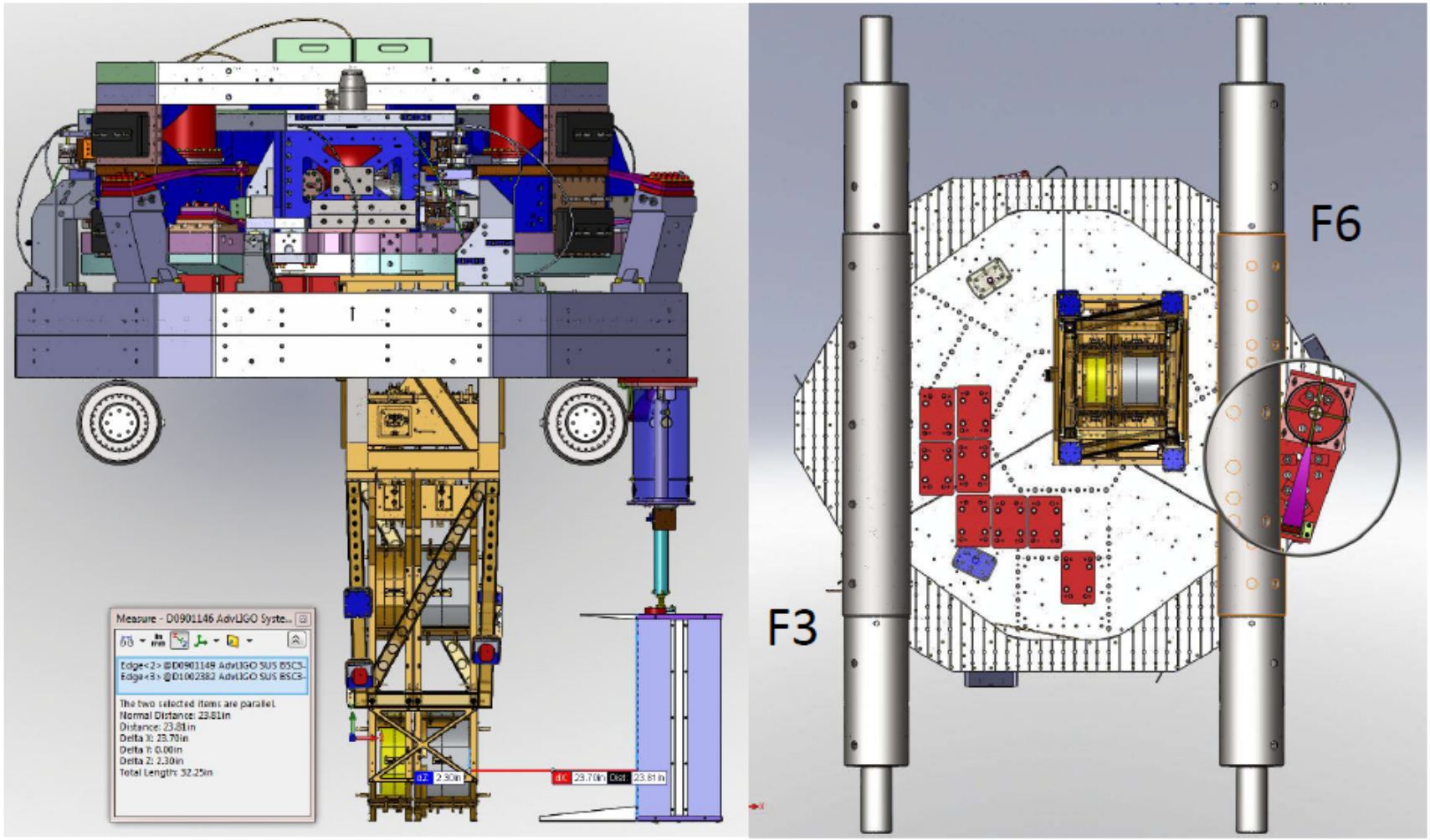

Figure 37: Arm Cavity Baffle Installed in BSC3-H1

- BSC5-H2 (D0900502)

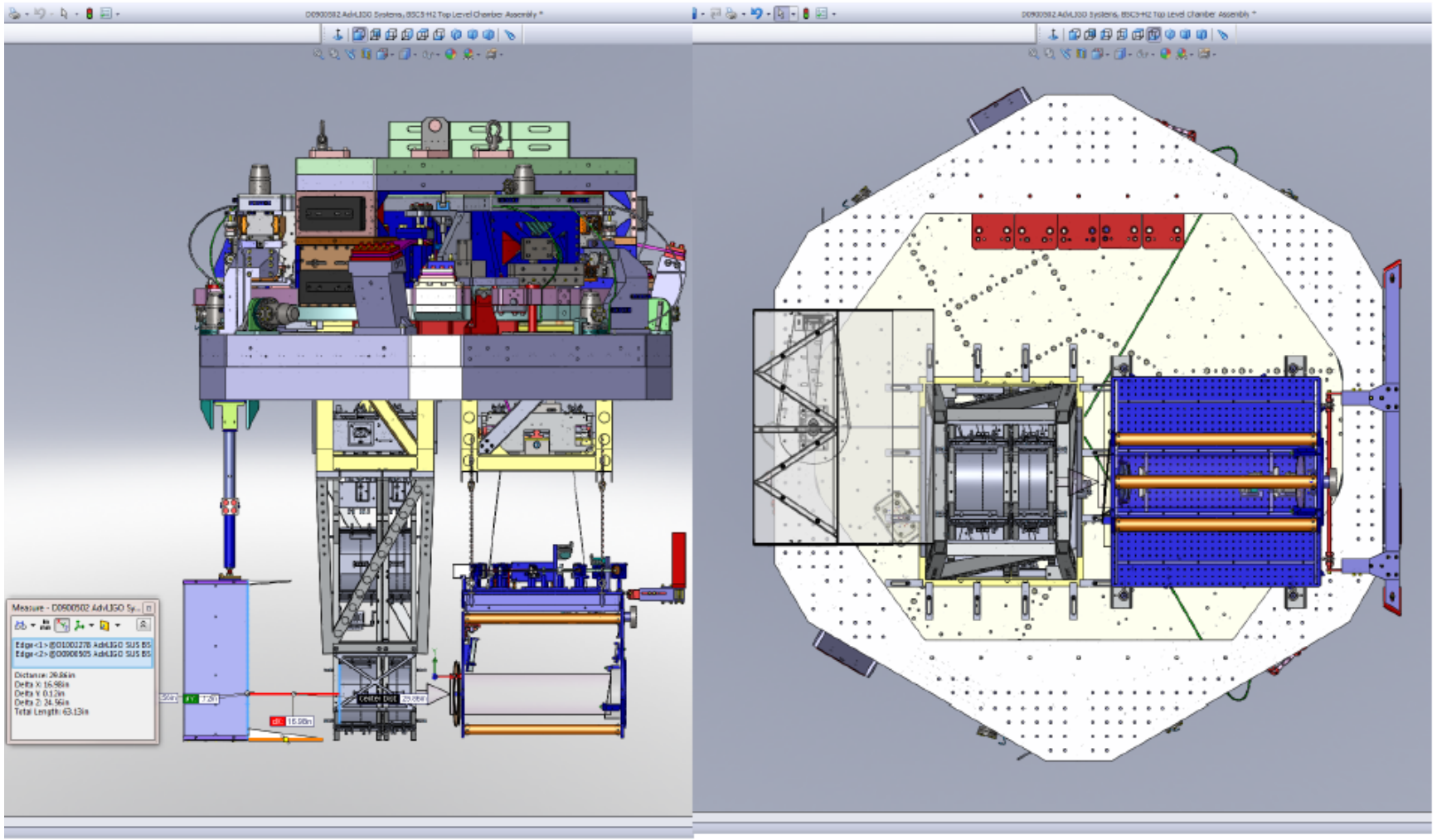

Figure 38: Arm Cavity Baffle Installed in BSC5-H2

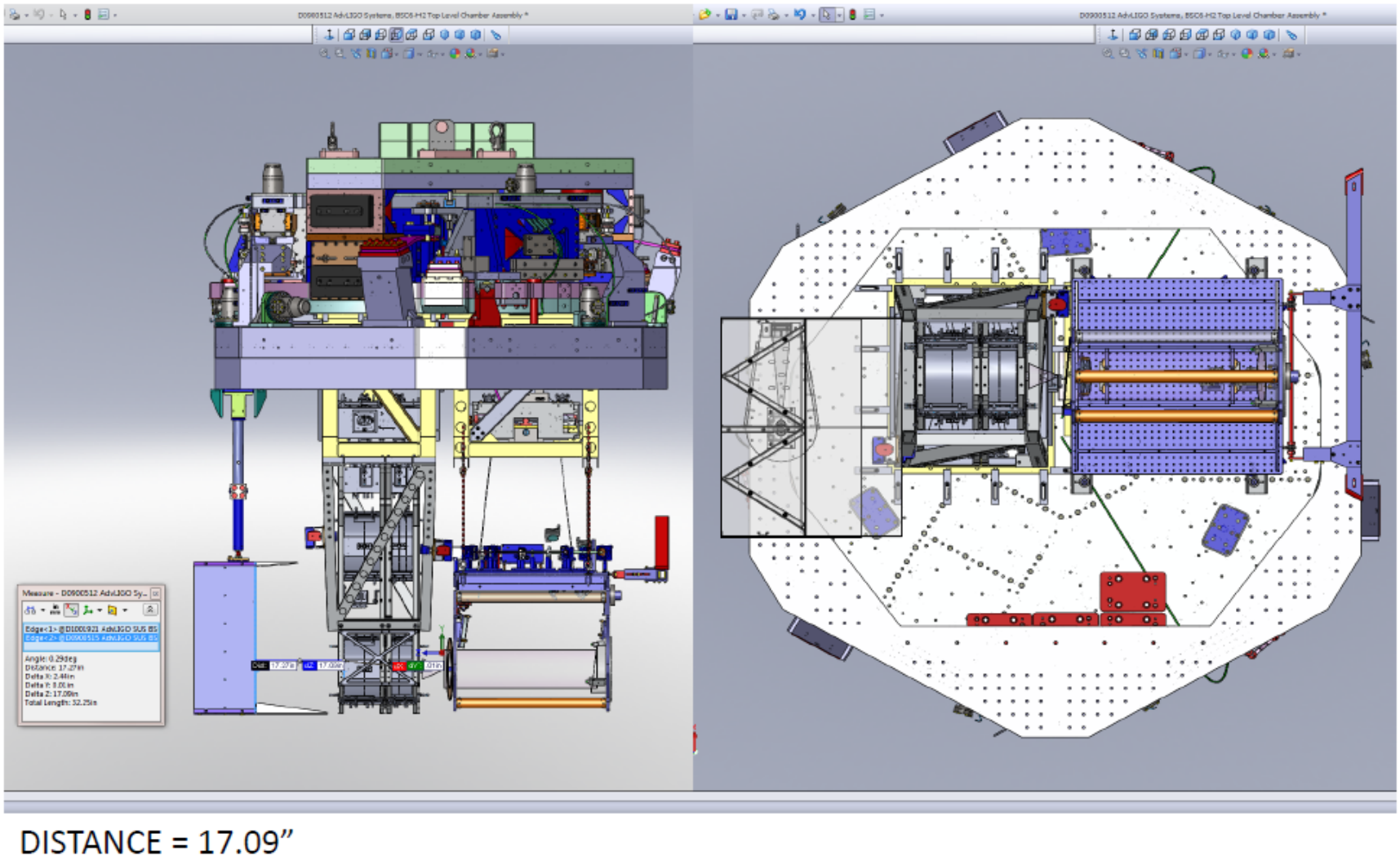

Figure 39: Arm Cavity Baffle Installed in BSC6-H2

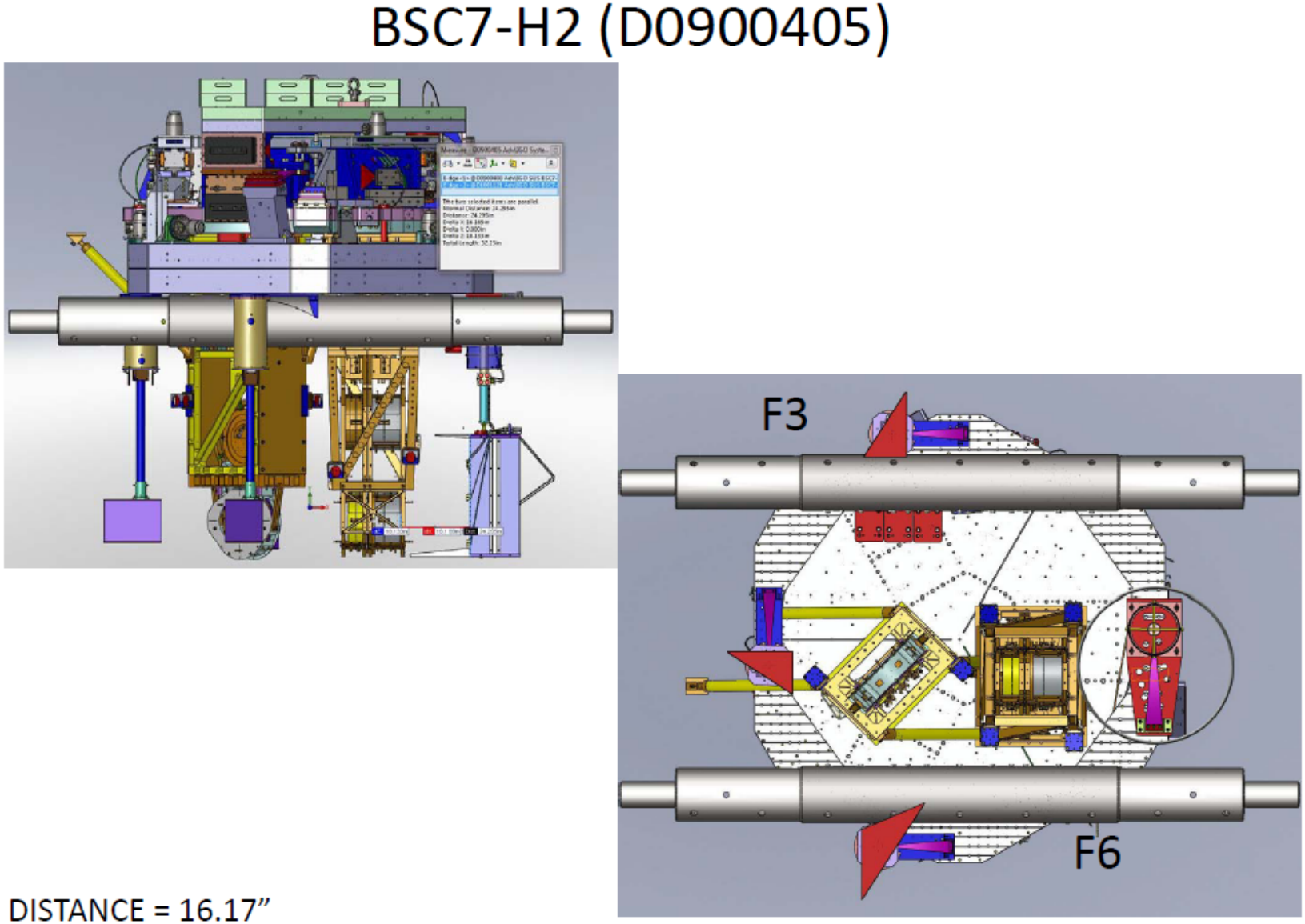

Figure 40: Arm Cavity Baffle Installed in BSC7-H2

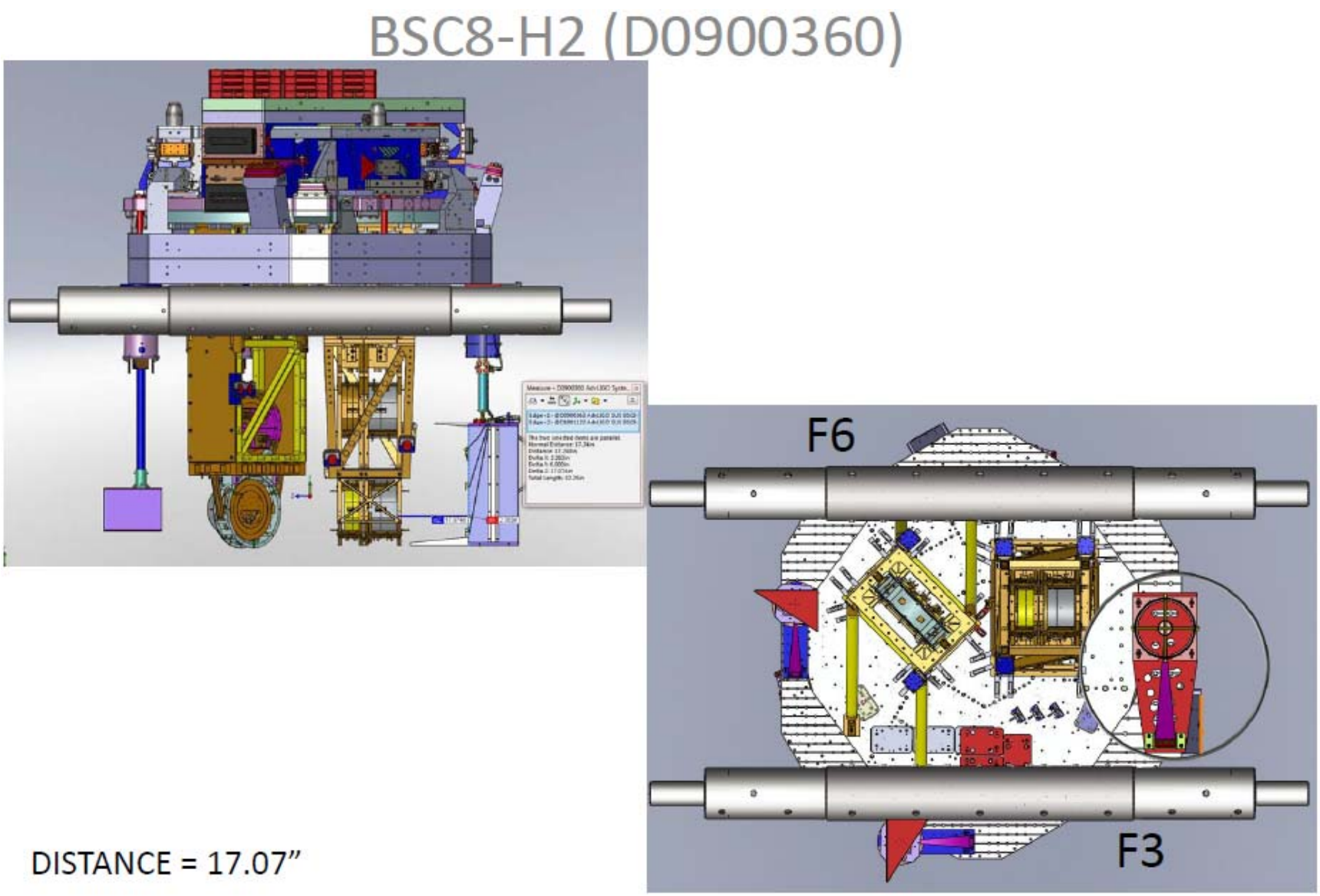

Figure 41: Arm Cavity Baffle Installed in BSC8-H2

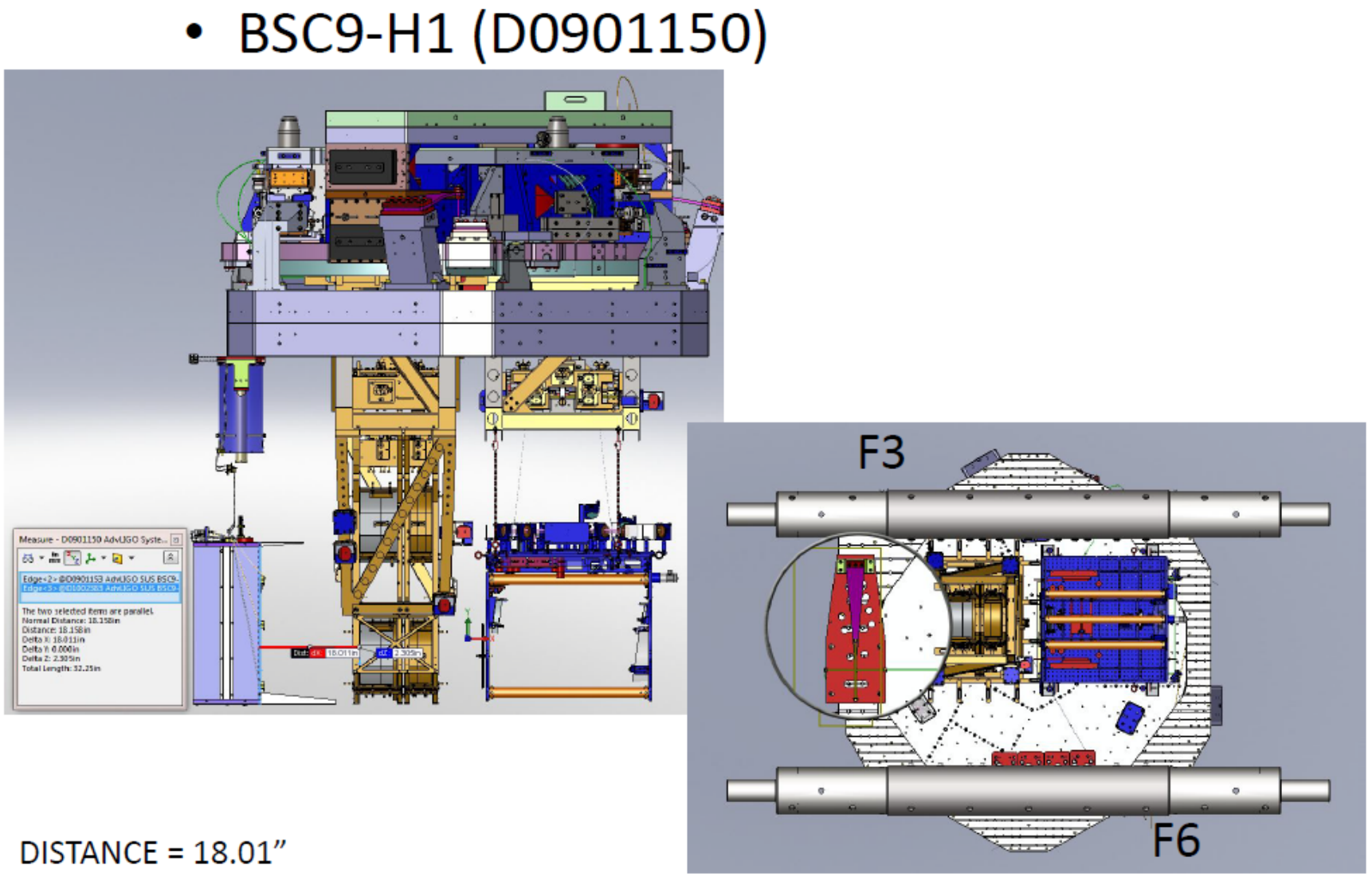

Figure 42: Arm Cavity Baffle Installed in BSC9-H1

- BSC10-H1 (D0901154)

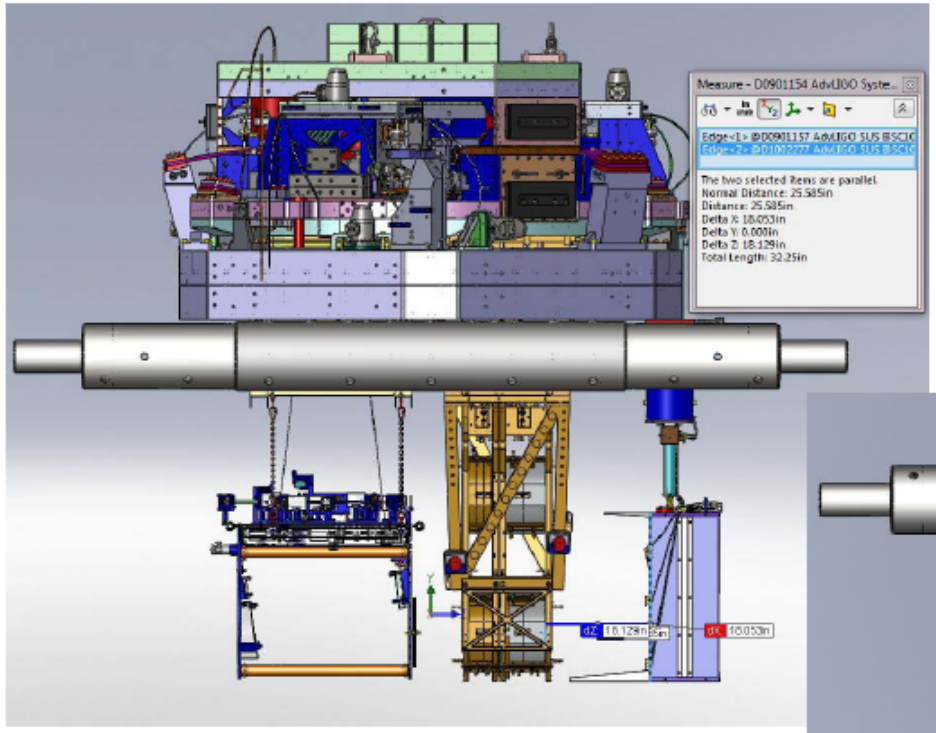

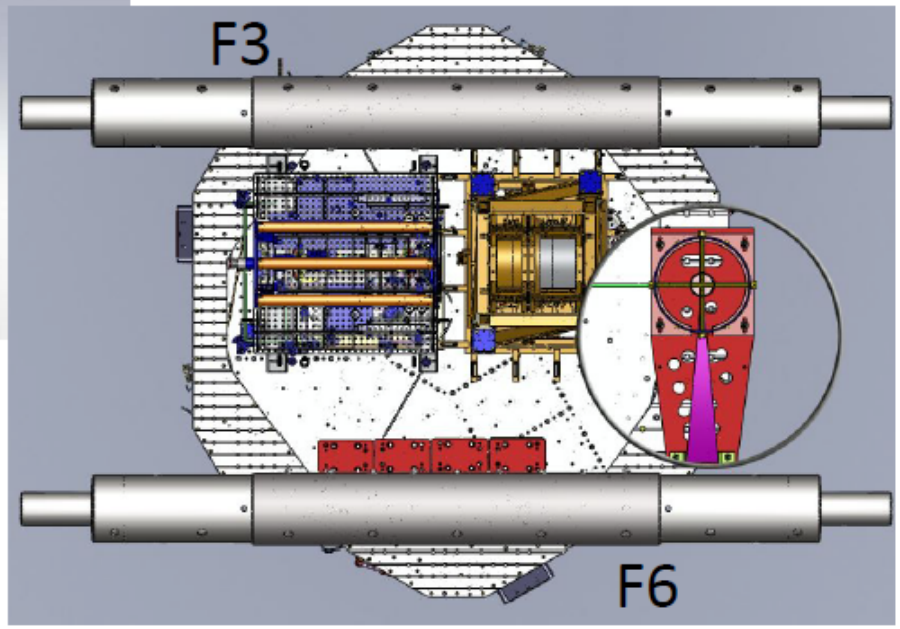

DISTANCE = 18.05”

Figure 43: Arm Cavity Baffle Installed in BSC10-H1

The Figure 44 shows the detail of the Arm Cavity Baffle suspension interface plate clamped to the Stage 0; the support plate has been made transparent so that the down tube mounting plate and other details of the baffle suspension that hang below the transparent suspension support plate can be seen. In particular, a mounting access slot is located near the center of the down tube where a clamp can be positioned to minimize the bending of the suspension support plate due to the weight of the down tube assembly; other clamps attach to available mounting holes in the Stage 0.

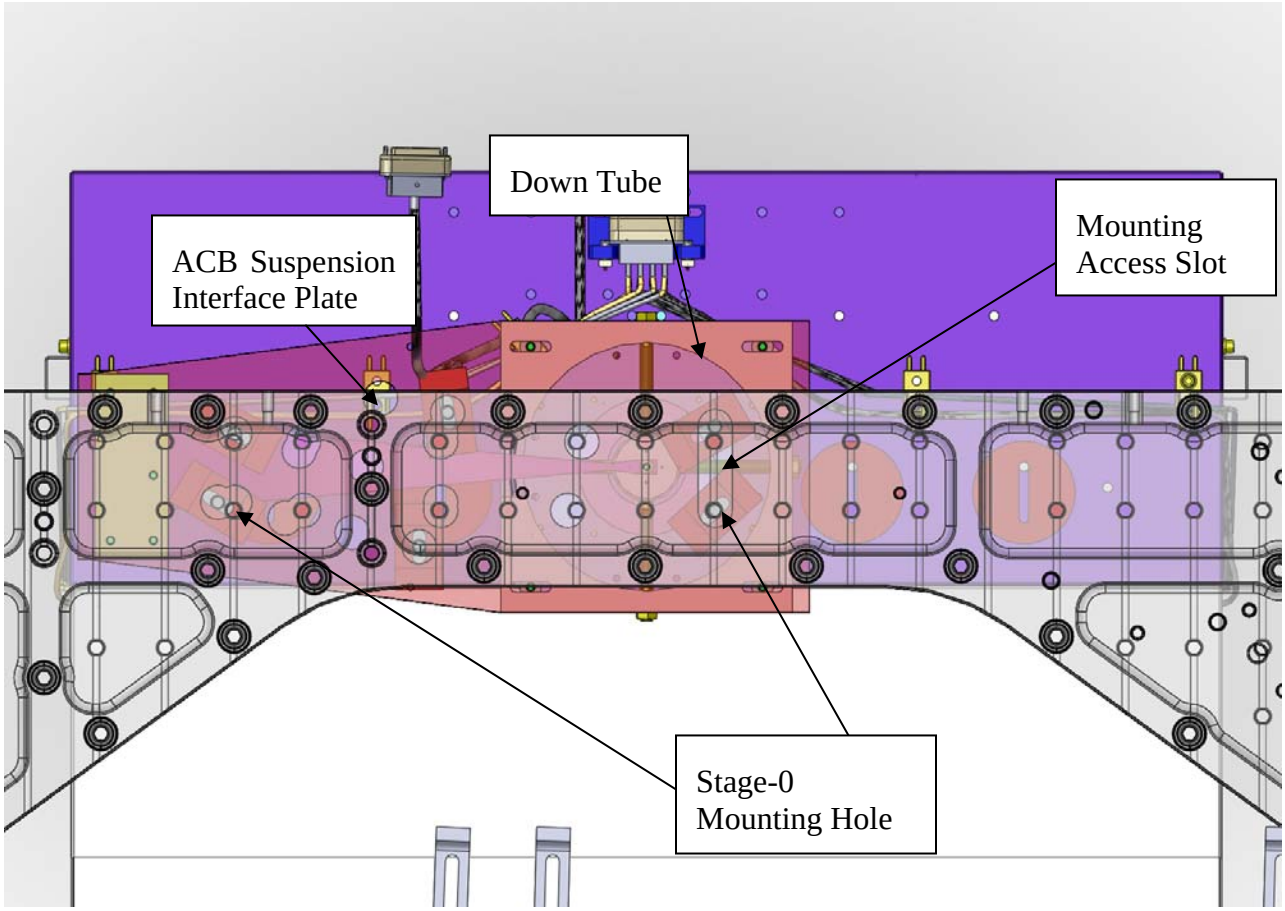

Figure 44: Detail of Arm Cavity Attachment to Stage 0

Further detail of the clamping arrangement is shown in Figure 45.

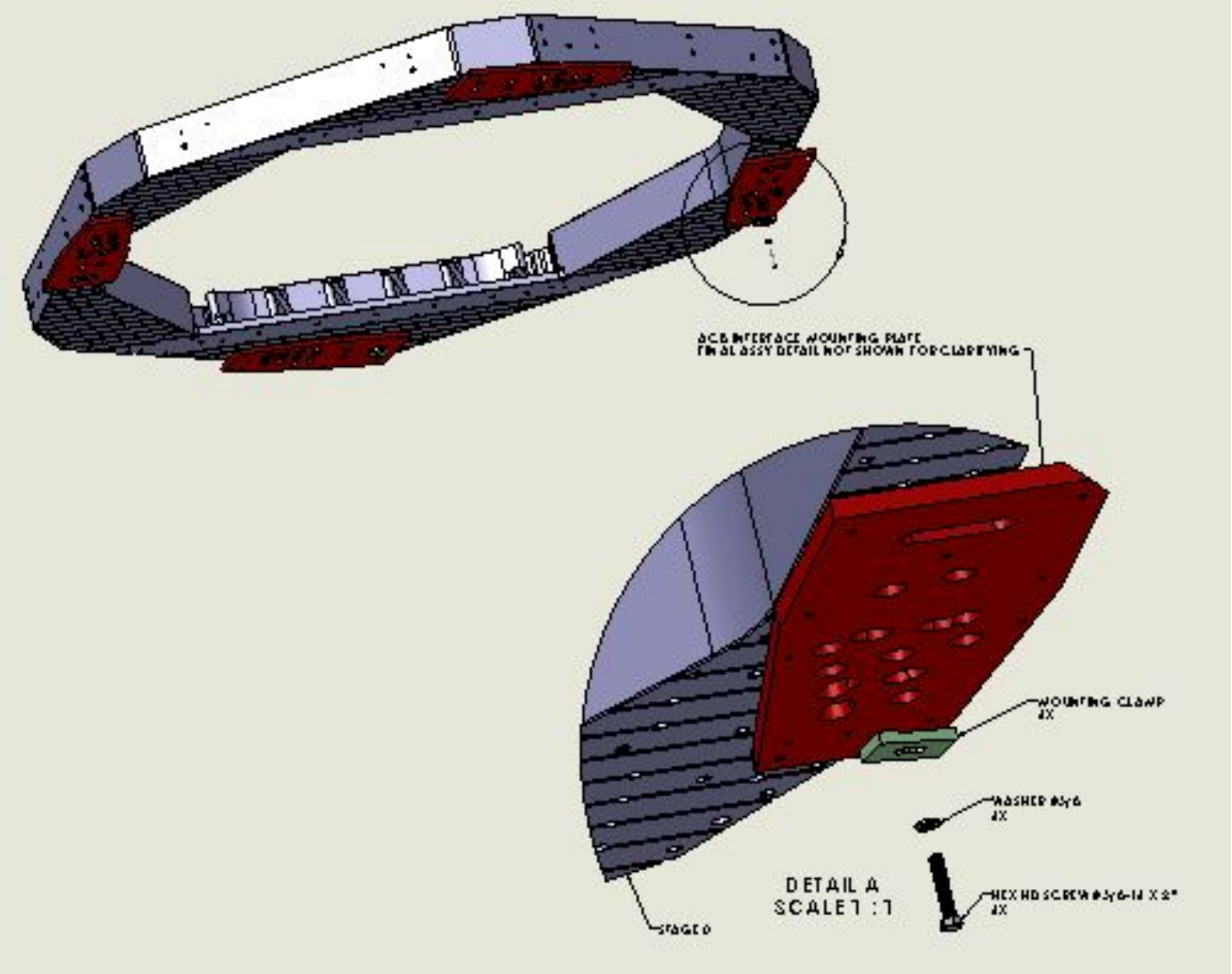

Figure 45: Detail of support plate clamp attachment

5.4 Stay Clear Margin

5.4.1 Concentricity with Center of ITM & ETM

The aperture of the Arm Cavity Baffle is 346 mm, which is larger than the 340 mm diameter of the ITM and ETM COC, and the ACB will not cause a power loss of the arm cavity beam. The aperture will be aligned concentric to the COC within 4 mm.

5.4.2 Proximity to the ITM & ETM Quad Suspension Structure

The ACB wide angle scatter box will be set to protrude to within 2 inches from the quad suspension structure facing the ACB.

5.5 Electrical Interfaces

The ALS photo detector electrical power and signal cables will be terminated at the internal vacuum feed through in the BSC chamber, as described in D1002870, Flange Layout, Cable Lengths, Bracket Location and Related Input Documents. The internal feed through connection is the interface between AOS and ISC--AOS is not responsible for cabling outside the vacuum chamber

.